Interaction Notes

Note 409

May 1981

Singularity Expansion Method Parameter Measurement

C. A. Lin
J. T. Cordaro
The University of New Mexico
Albuquerque, New Mexico 87131

ABSTRACT

The natural frequencies, natural modes, and coupling coefficients are computed for a wire model of an aircraft. These same parameters are calculated from scale model measurements made at the University of Michigan and from system level aircraft test data obtained from the ATHAMAS I, ATHAMAS II, and ATLAS I electromagnetic pulse simulators. Comparisons are made between the wire model theoretical results and the results from the various measurements.

The authors express their appreciation to Carl E. Baum of the Air Force Weapons Laboratory for several helpful discussions on SEM and to K. S. Cho for providing several numerical results.

TABLE OF CONTENTS

LIST OF FIGURES

LIST OF FIGURES (continued)

LIST OF FIGURES (continued)

CHAPTER 1

INTRODUCTION

During electromagnetic pulse (EMP) testing surface currents are induced on the skin of an aircraft. These currents are measured at a number of different locations on the aircraft. Then the measurements are repeated with the aircraft in different orientations relative to the incident field. The resulting data are a collection of short duration (typically 2 to 5 μsec) time functions. When the test results are interpreted, comparisons are made between measured and predicted currents. The predicted currents consist of computer code results and scale model measurements. Usually these comparisons are made by overlaying time or frequency domain graphs. The process of collecting and storing measurement data and of comparing them with predictions could be improved greatly if the information in the surface currents could be condensed in some way. The singularity expansion method (SEM) offers this possibility for improvement.

The SEM introduced by Baum [1] provides a compact and physically meaningful way of characterizing a conducting body's response to EMP. With this method the response of a conducting body to an incident impulse plane electromagnetic wave is expressed as a sum of complex exponentials. This sum depends on a few parameters, namely natural frequencies, natural modes, coupling coefficients, and normalization factors. If these parameters are known the response to an arbitrary plane wave excitation can be obtained. Conversely, the

parameters can be calculated from a sufficient quantity of surface current responses plus knowledge of the incident field. In principle, it is possible to take a large number of surface current measurements and compress the information contained in them into a few tables and graphs of SEM parameters. This report addresses some of the practical problems in carrying out this data compression process. There are two problem areas to consider. First, the SEM parameters should be calculated for some aircraft model. Second, the parameters should be calculated from measured data and compared with the theoretical model results.

The first of these problems has been considered by several investigators. Because of the complexity of aircraft surface geometry, it is difficult to formulate and solve the scattering problem for an exact aircraft model. As a consequence, simplified models have been used to allow tractable mathematical formulations which preserve the global aircraft features. Crow et al. [2] used perpendicular crossed wires as an aircraft model. They divided the wires into segments and assumed sinusoidal current distribution along each segment. Then they obtained an analytic expression for the scattered electric field in terms of induced current. Based on the Pocklington integral-differential equation and the boundary conditions of the incident and scattered electric fields, a matrix equation relating induced current and incident electric field was formed by means of method of moments. The zeros of the determinant of the system matrix defined the locations of natural frequencies. They were found numerically by Muller's method. The natural modes and coupling

coefficients were also defined, and solved for numerically [3]. In subsequent work these results were extended to the case of crossed wires over a perfectly conducting ground plane [4] and then the imperfect ground case [5]. The latter study is based on transmission line theory and is much simpler than the conventional method of moment techniques.

Bedrosian [6] developed the "six length stick model" and computed natural frequencies and natural modes for several different types of aircraft. The stick model employed the assumption of a sinusoidal current distribution on each conducting stick. At the junctions conservation of the current and continuity of charge-density were enforced. A matrix equation was developed for the junction and end conditions on the sticks. The zeros of the determinant of the matrix and the computation of average radiated power and stored magnetic energy for each cycle yielded the natural frequencies. The natural modes were obtained from the matrix equation.

In the first part of the work described in this report a simple wire model of a B-52 aircraft was analyzed. The wire current was calculated using a time domain computer code. The SEM parameters for this simple model were computed from the current. These results are compared below with the results given in [2] and [6]. Of course one would hope that these wire model parameters would compare reasonably well with the actual (but unknown) B-52 aircraft SEM parameters.

The second part of our work consisted of an attempt to calculate the parameters from measured data. Two types of measured B-52 data were available. Frequency response data for a B-52 scale

model has been taken at the University of Michigan Radiation Laboratory by Liepa [7]. Also, some surface current density measurements from B-52 system level tests conducted at the ATHAMAS I (HPD), ATHAMAS II (VPD), and ATLAS I (Trestle) Simulator facilities were obtained. None of these measurements were taken with SEM parameter extraction as a goal. Consequently there are not enough measurements to completely define the SEM description. But the results are encouraging and indicate that the parameters can be determined from experimental data.

A description of the wire model and the method of calculating the SEM parameters is presented in Chapter 2. Chapter 3 gives the numerical results and their comparison. Chapter 4 presents conclusions drawn from this study. Two techniques for calculating the "sum of complex exponentials" description for a transient waveform, Prony's method and the iterative premultiply method, are treated in detail in the appendix.

CHAPTER 2

FORMULATION

2.1 GENERAL EXPRESSION FOR THE RESPONSE

In this report no attempt is made to determine or analyze the current density variation around the circumference of the aircraft body. There are two reasons for this. First, the test data are surface current density measurements but the measurements are not distributed around the circumference in any consistent way. Second, the thin wire code computes the total axial current on wire segments. Any current variation about the wire circumference is ignored in making the thin wire approximation. For these reasons the surface current is modeled below as having a two rather than three-dimensional space dependence.

Consider a scatterer lying in the xy plane in three-dimensional space struck by a plane electromagnetic wave. The direction of the propagation $\vec{k}$ of the incident field makes an angle ϕ with the z-axis and the projection of $\vec{k}$ on the xy plane makes an angle θ with the x-axis. Then using the SEM representation [1], the induced current at any location on the scatterer can be written as

$$I(t,\theta,\phi,x,y) = \sum_{\alpha} R_{\alpha}(\theta,\phi,x,y)\, \exp(s_{\alpha}t)u(t - t_{o}) + g(t,\theta,\phi,x,y) \qquad (1)$$

where t_o is the turn on time, the s_α are the natural frequencies or poles of the scatterer, the R_α are the corresponding residues at s_α

and $g(t,\theta,\phi,x,y)$ is the forced response. The summation over α represents the natural response of the scatterer. It is shown in [1] that the residues can be factored as

$$R_\alpha(\theta,\phi,x,y) = \eta_\alpha^{max}\ \eta_\alpha^1\ (\theta,\phi) i_\alpha(x,y)\tilde{f}(s_\alpha) \qquad (2)$$

where

η_α^{max} - the normalization factor

η_α^1 - normalized coupling coefficient

i_α - normalized natural mode

$\tilde{f}(s_\alpha)$ - Laplace transform of the exciting function.

As a result, the natural response can be expressed in terms of SEM parameters as

$$\sum_\alpha R_\alpha(\theta,\phi,x,y)\exp(s_\alpha t)\ u(t - t_0)$$

$$= \sum_\alpha \eta_\alpha^{max}\ \eta_\alpha^1\ (\theta,\phi) i_\alpha(x,y)\tilde{f}\ (s_\alpha)\exp(s_\alpha t)u(t-t_0) \qquad (3)$$

Since the values of the induced current are always real, the poles s_α shown in Equation 1 occur in complex conjugate pairs or lie on the real axis of the complex s-plane. The pole locations depend on the geometry of the scatterer.

The natural modes describe the spatial amplitude variation in the current. They are normalized so that at the maximum magnitude points they are real and equal to one. They are independent of the angles of incidence θ and ϕ, but are functions of the spatial coordinates x and y. The coupling coefficients describe the coupling

between the incident field and the scatterer. They depend on the angles θ and ϕ, and are independent of x and y. They are also normalized so that at the maximum magnitude points they are real and equal to one. The normalization factors are calculated to provide proper magnitude and phase in Equation 3.

One of the greatest advantages of SEM in data compression is the factoring of the residues in Equation 2. Without Equation 2, it would appear that to define the surface current natural response it would be necessary to measure $I(t,\theta,\phi,x,y)$ at a large number of separate values of the argument. But from Equation 3, it is necessary to measure only enough data to define the product. The natural modes and coupling coefficients are usually well-behaved functions. This also reduces the number of the spatial samples. The natural frequencies along with other SEM parameters provide extrapolation in time and interpolation in spatial coordinates. The information in the surface current is then effectively condensed.

2.2 THE COMPUTING METHOD

Suppose $I(t,\theta,\phi,x,y)$ is known for $t \geq t_o$ and a number of θ,ϕ,x, and y values. In order to find the parameters, it is necessary to find the s_α and $R_\alpha(\theta,\phi,x,y)$ in Equation 1. Prony's method [8] was used to compute the natural frequencies and residues from the time domain response generated by the thin-wire code. This method is suitable for computer generated data. It does not work well with experimental data because of noise. For this reason the iterative premultiply method [9], [10] was used to analyze the Michigan scale

model and system test data. Both methods fit the given data by a sum of complex exponentials. Due to numerical error and measurement noise, there exist extra "fitting poles" that are not the poles of the response. However, the poles of the response can be recognized by increasing the number of complex exponentials fitted. As the order increases, some pole values become approximately constant to several decimal places while others change randomly. The poles that stabilize as the fitted order increases are the natural frequencies of the current data. The residues were obtained by a standard least-square curve fitting scheme, using the complex exponentials of the poles as a set of basis functions. For field excitations that can be expressed as a sum of complex exponentials, the poles and residues can be calculated from the source driven region where the exciting waveform is still present. For those which cannot, it is useful to wait until the forced response dies out essentially.

The result of applying one of the two methods to the response data is a collection of s_α and $R_\alpha(\theta,\phi,x,y)$ values. The pole values calculated from different data sets should vary only within a few percent. The α natural mode is calculated by fixing θ and ϕ and scaling the α residue variation as x and y are changed. This is done for each particular natural frequency. By Equation 2, the natural modes calculated should be independent of the incident angles θ and ϕ. However, because of computation and/or measurement error, some dependence exists. In order to reduce the effect of these errors, the field orientation that yielded maximum residues was chosen. For the natural frequency s_α, there exists a location on the aircraft that

makes the corresponding R_α greater than that of other locations for any field orientation. In the calculation of the α-coupling coefficient, this particular location was chosen. Then the variation in R_α as a function of θ,ϕ was tabulated and normalized to yield the α-coupling coefficient, $\eta_\alpha^1(\theta,\phi)$. From Equation 2, the α-normalization factor can be expressed as

$$\eta_\alpha^{max} = \frac{R_\alpha(\theta,\phi,x,y)}{\eta_\alpha^1(\theta,\phi) i_\alpha(x,y) \tilde{f}(s_\alpha)} \tag{4}$$

In actual calculation only

$$R'_\alpha(\theta,\phi,x,y) = R_\alpha(\theta,\phi,x,y) \exp(s_\alpha t_1) \tag{4a}$$

is available, where t_1 depending on the starting point t_s in the calculation of poles and residues, and the distance D_o between the incident wavefront and the origin of the coordinate system.

2.3 DESCRIPTION OF DATA

2.3.1 The Thin-Wire Code Data

The wire model of the B-52 aircraft consisted of three equal radius cylinders. The radius R = 1.6 meters was chosen so that the cylinders and the B-52 fuselage would have approximately the same cross-sectioned area. The locations of the cylinders are shown in Figure 1. The incident plane wave is depicted in Figure 2. The direction of propagation $\vec{k}$ makes an angle θ with z-axis, and the projection of $\vec{k}$ on the xy plane makes an angle ϕ with the x-axis, η is the polarization angle of the incident electric field, and only η = 90° is considered in the simulation. At t = 0, the wavefront of the

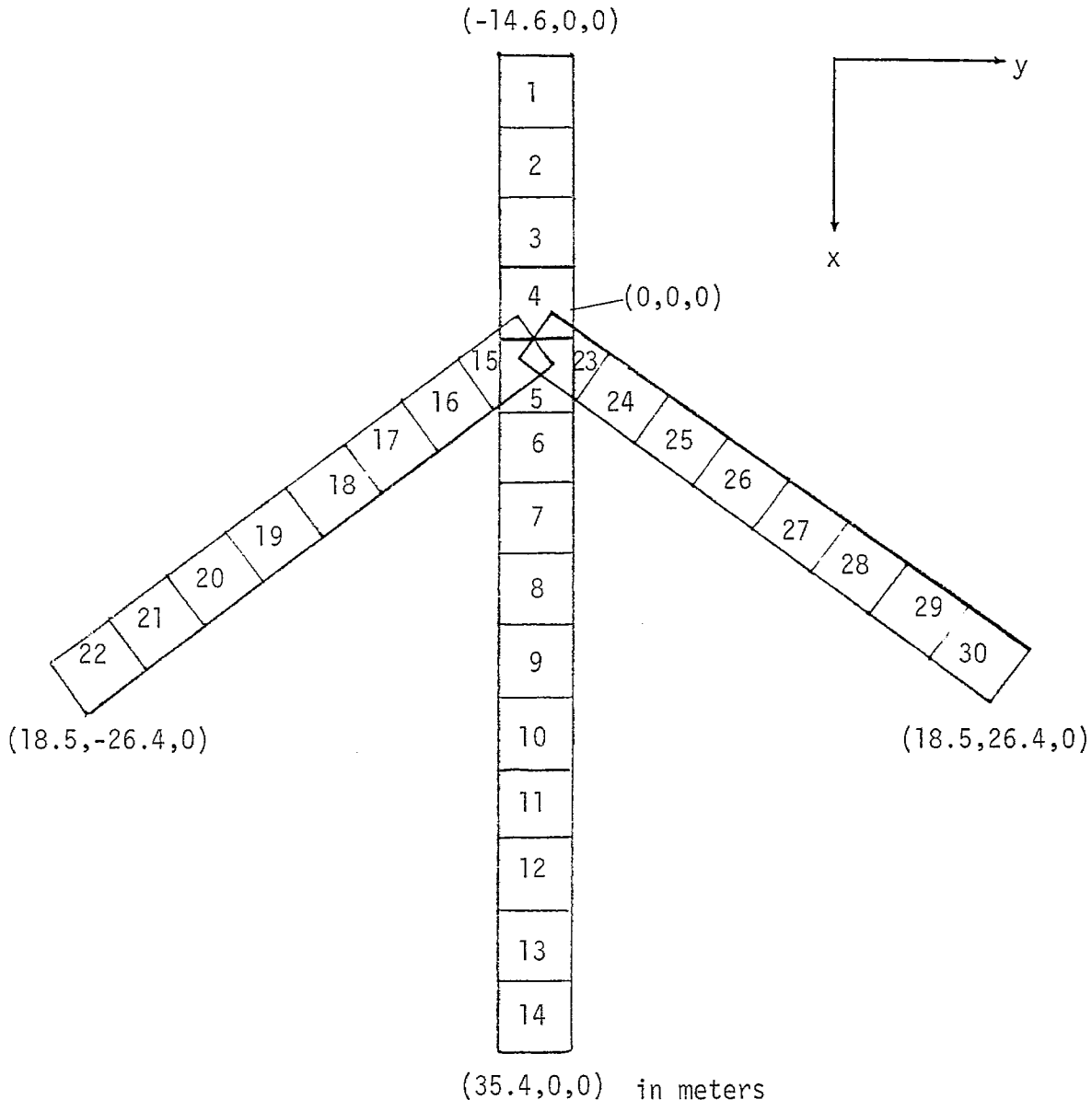

Figure 1. The segmented wire model of B-52.

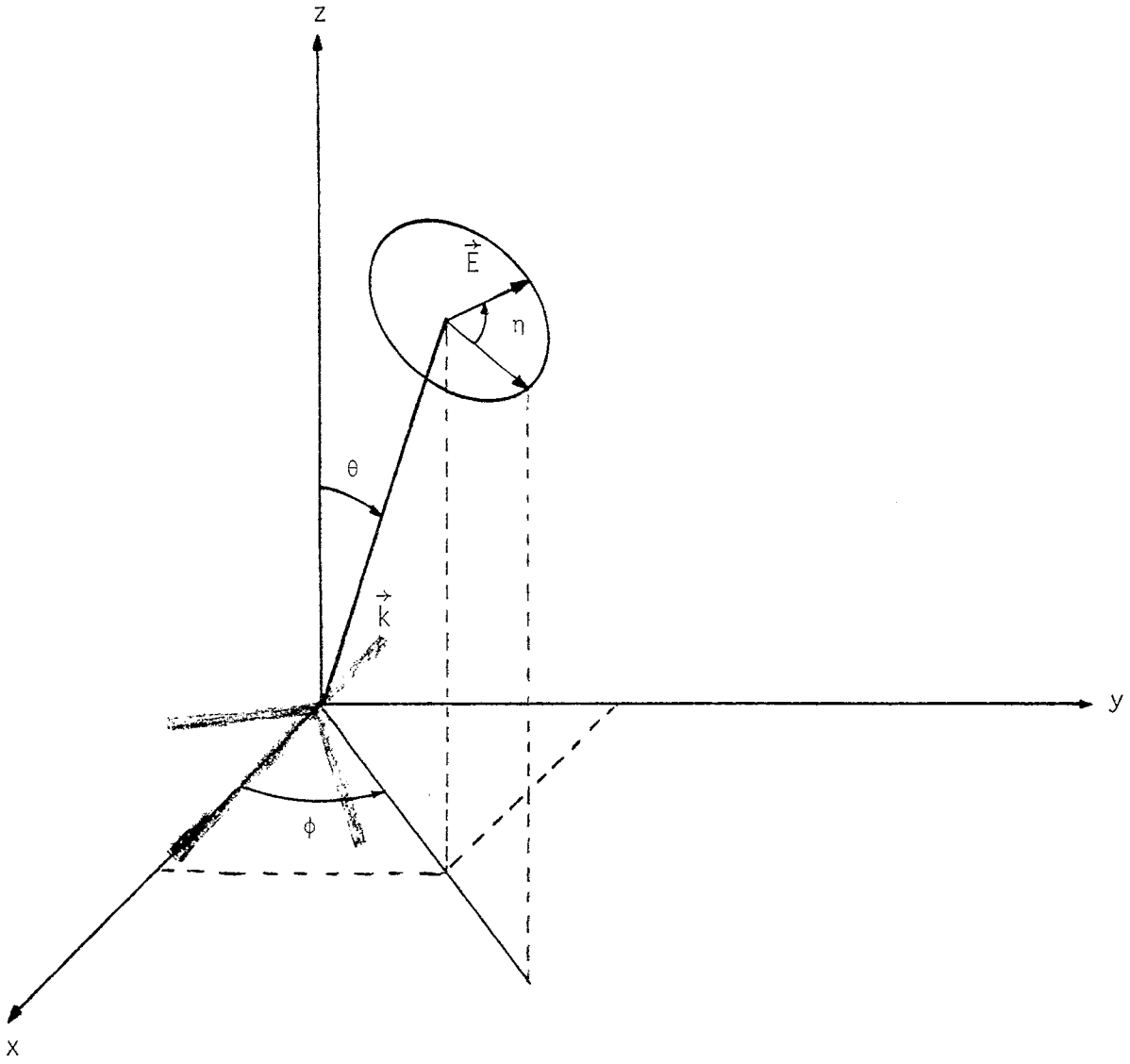

Figure 2. The coordinate system and electric field orientation.

incident wave is assumed to be a distance of D from the origin of the coordinate system, where D_0 = 40 meters. A double exponential pulse electric field

$$E(t) = E_0 \cdot f(t)$$
$$f(t) = \exp(-\alpha t) - \exp(-\beta t), \qquad t \geq 0$$
$$= 0 \qquad \text{otherwise} \qquad (5)$$

was used as the incident electric field, where $\alpha = 4 \times 10^6$, $\beta = 2.2 \times 10^8$, and E_0 = 1 volt/meter.

The thin wire code solves the time-domain electric field integral equation numerically [11], [12]. The numerical solution begins by approximating the structure geometry by a set of cylindrical segments. Then the integral equation is rendered into a set of linear equations by the method of moments. For any desired incident field, the equations are treated as an initial value problem and total axial current is obtained for each time step and each segment. In this study, the wire model was divided into 30 segments as shown in Figure 1. The time step was chosen as $\Delta t = 2 \times 10^{-8}$ sec. For each run of the thin-wire code, the axial currents are available for 600 time steps at each of the 30 segments.

In the first stage of our study, we also experimented with the wire model with the tail included. The frequency responses from both models were compared to the frequency response of the Michigan scale model data. The data from the model matched the Michigan scale model data no better than that from the present model in the high frequency region (above 6 MHz), while they all were close to each other in the low frequency region. This is the reason for adopting the present

wire model for simulation.

2.3.2 The Michigan Scale Model Data

The experiment performed at the University of Michigan was that of illuminating a scale model B-52 by an electromagnetic plane wave. Surface current density at several locations on the model was measured and scaled to full B-52 aircraft dimensions. The measured current density data consist of the frequency response at several locations along the fuselage and wings for five different field excitations. The field orientations, in terms of the definition in Figure 2, are

orientation 1: $\theta = 90°$, $\phi = 90°$, $\eta = 90°$

orientation 2: $\theta = 0°$, $\phi = 180°$, $\eta = 90°$

orientation 3: $\theta = 90°$, $\phi = 90°$, $\eta = 180°$

orientation 4: $\theta = 90°$, $\phi = 90°$, $\eta = 90°$

orientation 5: $\theta = 90°$, $\phi = 180°$, $\eta = 90°$

Before the calculation of SEM parameters from these data, the Inverse Fourier transform was performed to get time domain responses. A second-order Butterworth low-pass filter with cutoff frequency of 10 MHz was applied to filter out the high frequency components

$$(H(s) = \omega_o^2/(s^2 + 1.414\ \omega_o s + \omega_o^2),\ \omega_o = 2\pi \cdot 10^7).$$

2.3.3 System Test Data

The measured current data from the ATHAMAS I (HPD) simulator consist of data sets measured at three different locations on the fuselage and one data set measured on the wing. In this test a B-52 aircraft was placed on a lossy ground and illuminated by an EMP with the principal component of the electric field either parallel or perpendicular to the fuselage. The field orientations correspond

roughly to orientations 1 and 2 for the Michigan data except that $\theta \simeq 45°$ in each case. Because of the lossy ground plane, the aircraft poles extracted from these data are expected to have more negative real parts than those from that in free space case [5]. In the ATHAMAS II (VPD) simulation the ground plane is more conductive, and the incident electric field is perpendicular to the conducting ground plane. Only one current measurement is available. Poles extracted from these data are expected to be closer to the imaginary axis [4] than are the poles from the other data.

The data from ATHAMAS I and ATHAMAS II are time domain data. Each data record was filtered as above before poles and residues were calculated.

In the ATLAS I (TRESTLE) simulator, the measurement data consist of time responses measured at two different locations on the aircraft. The incident field orientations are the same as orientation 4 and orientation 5 in the Michigan test. The iterative premultiply method was applied to the digitized time domain waveforms.

CHAPTER 3

NUMERICAL RESULTS

3.1 EVALUATION OF SEM PARAMETERS FROM DATA GENERATED BY THE THIN WIRE CODE

3.1.1 The Transient Response and the Exciting Field

The 30 segment wire model shown in Figure 1 was formulated for the time domain thin wire computer code WT-MBA/LLL1B [13]. A double exponential pulse was selected as the exciting electric field. Plane wave excitation was assumed, and the field orientation was characterized by the angles θ and ϕ, as shown in Figure 2 with $\eta = 90°$. For each run of the thin wire code, the induced current data at the center of each of the thirty segments was computed at 600 time steps of width Δt, with $\Delta t = 2 \times 10^{-8}$ sec. The thin wire code was run repeatedly to generate current data for different field orientations. For an arbitrary incident plane wave, the electric field can be decomposed into two orthogonal components, one with the $\vec{E}$ field parallel to the fuselage (x-axis), the other with the $\vec{E}$ field perpendicular to the fuselage. These components are called symmetric excitation and antisymmetric excitation respectively [14].

3.1.2 The Natural Frequencies

Prony's method was applied to the current data to compute the poles and residues in Equation 1. The poles are the natural frequencies of the scatterer, and were determined by the criterion set in Section 2.2. Four pole-pairs were extractable from the current

induced on the fuselage, and one additional pole-pair appeared in the current data from the wing. These values are listed in Table 1.

Table 1. Natural frequencies of the B-52 wire model poles

α	poles	
1	as,1,1	$-0.145 \times 10^7 + j\ 0.135 \times 10^8$
2	sy,1,1	$-0.810 \times 10^6 + j\ 0.149 \times 10^8$
3	sy,1,2	$-0.312 \times 10^7 + j\ 0.196 \times 10^8$
4	sy,2,1	$-0.389 \times 10^7 + j\ 0.373 \times 10^8$
5	sy,3,1	$-0.328 \times 10^7 + j\ 0.408 \times 10^8$

It was observed that when the exciting field contained only the antisymmetric component, that is, $\vec{E}$ perpendicular to the fuselage, the first resonance dominated the current response on the wings. For this reason, the first mode is called the antisymmetric mode. The other four modes are called symmetric modes. The same mode designation is used as that used in [4].

3.1.3 The Natural Modes

Figures 3 through 7 present the real parts of the normalized natural modes for the five natural frequencies. It should be noted that for the antisymmetric mode only the distribution on the wings is shown, since no current is coupled to the fuselage. Three-dimensional plots of the natural modes are shown in Figures 8 through 10 with the arrow representing the direction of current flow. The imaginary parts of the natural modes are all small and hence, are not shown.

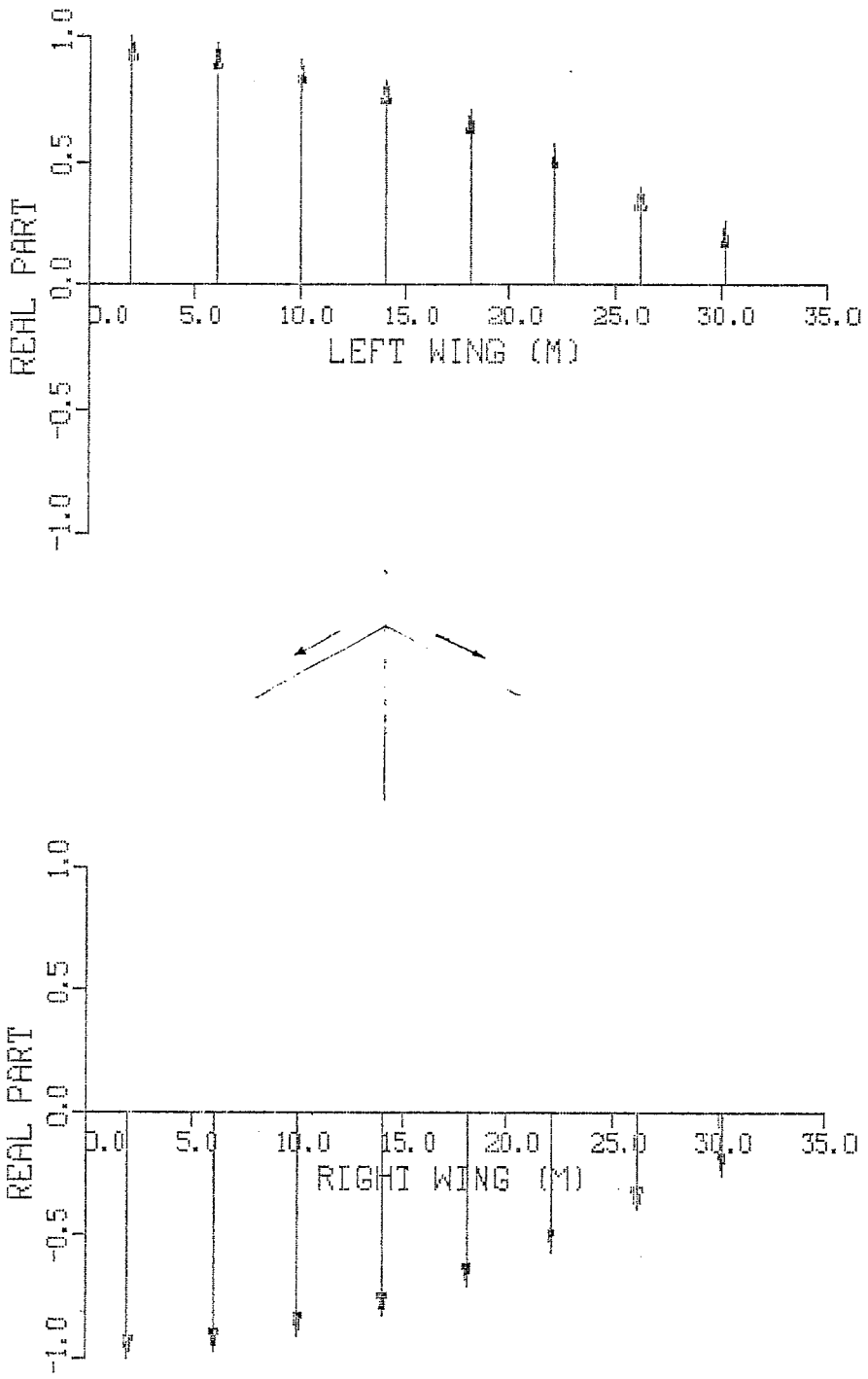

Figure 3. Real part of the first normalized natural mode.

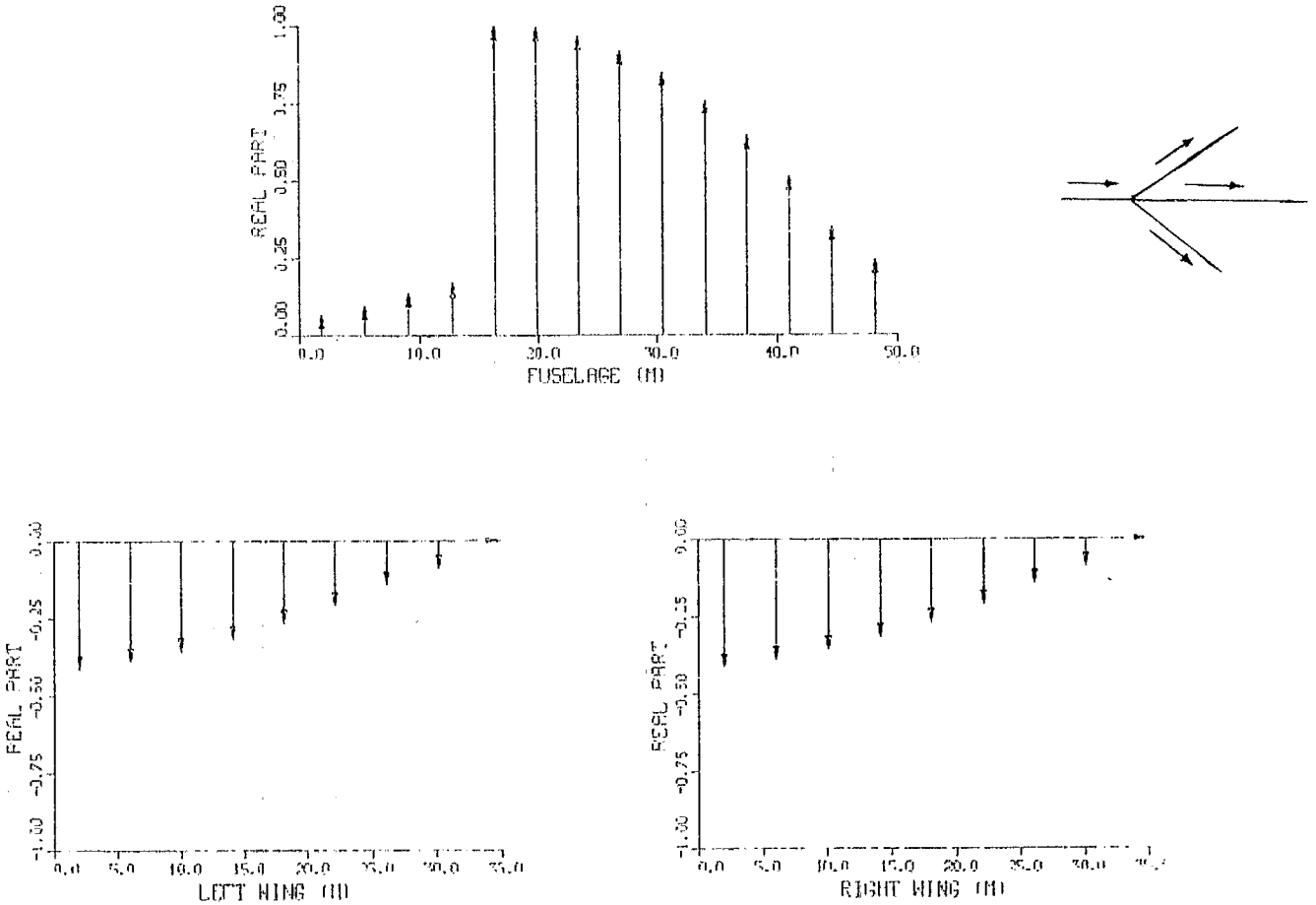

Figure 4. Real part of the second normalized natural mode.

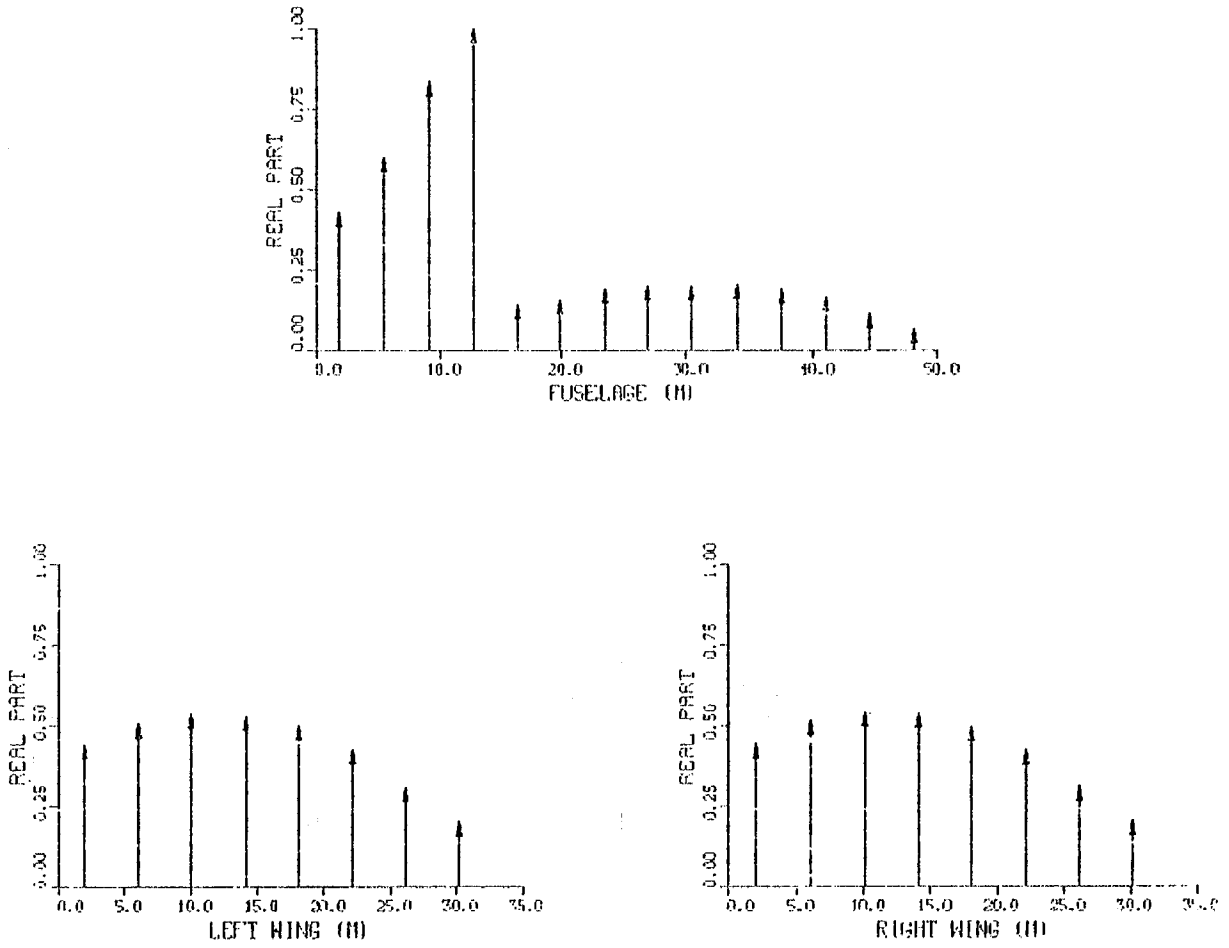

Figure 5. Real part of the third normalized natural mode.

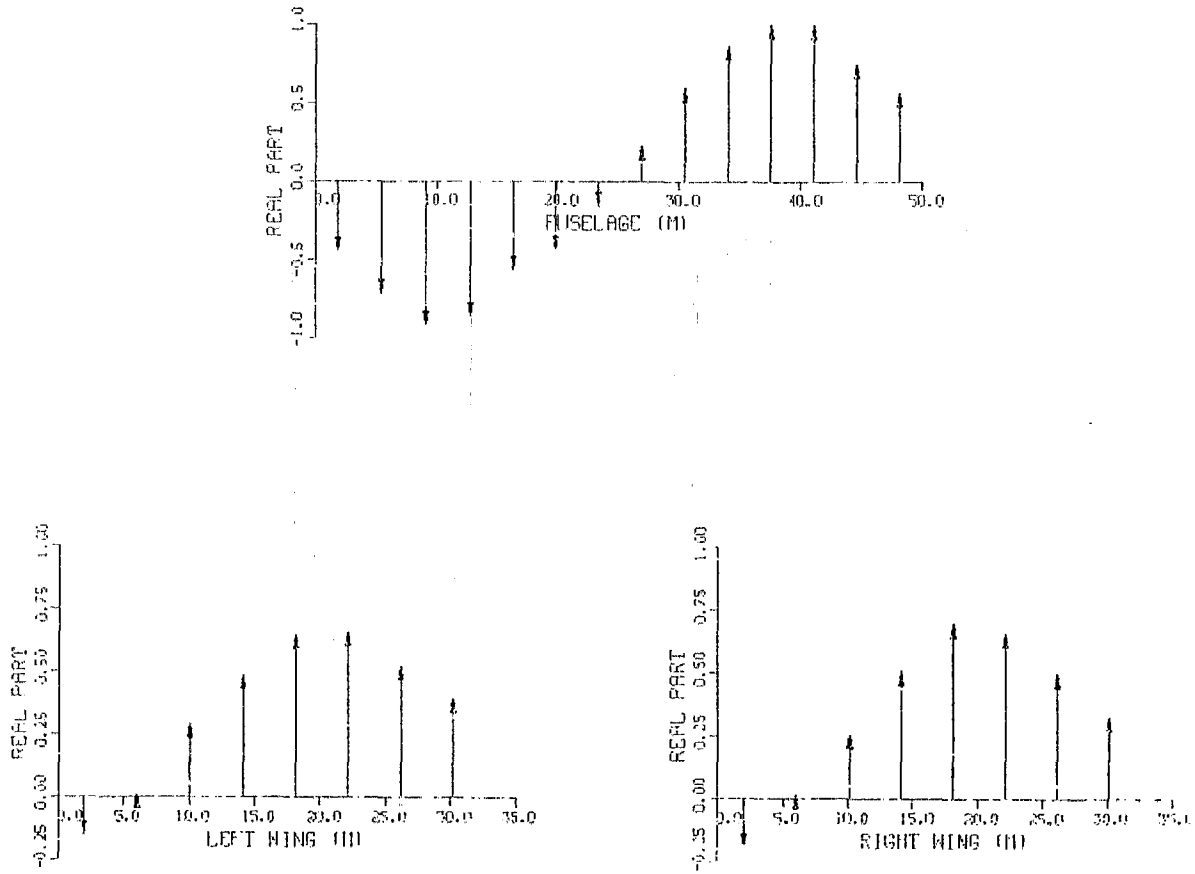

Figure 6. Real part of the fourth normalized natural mode.

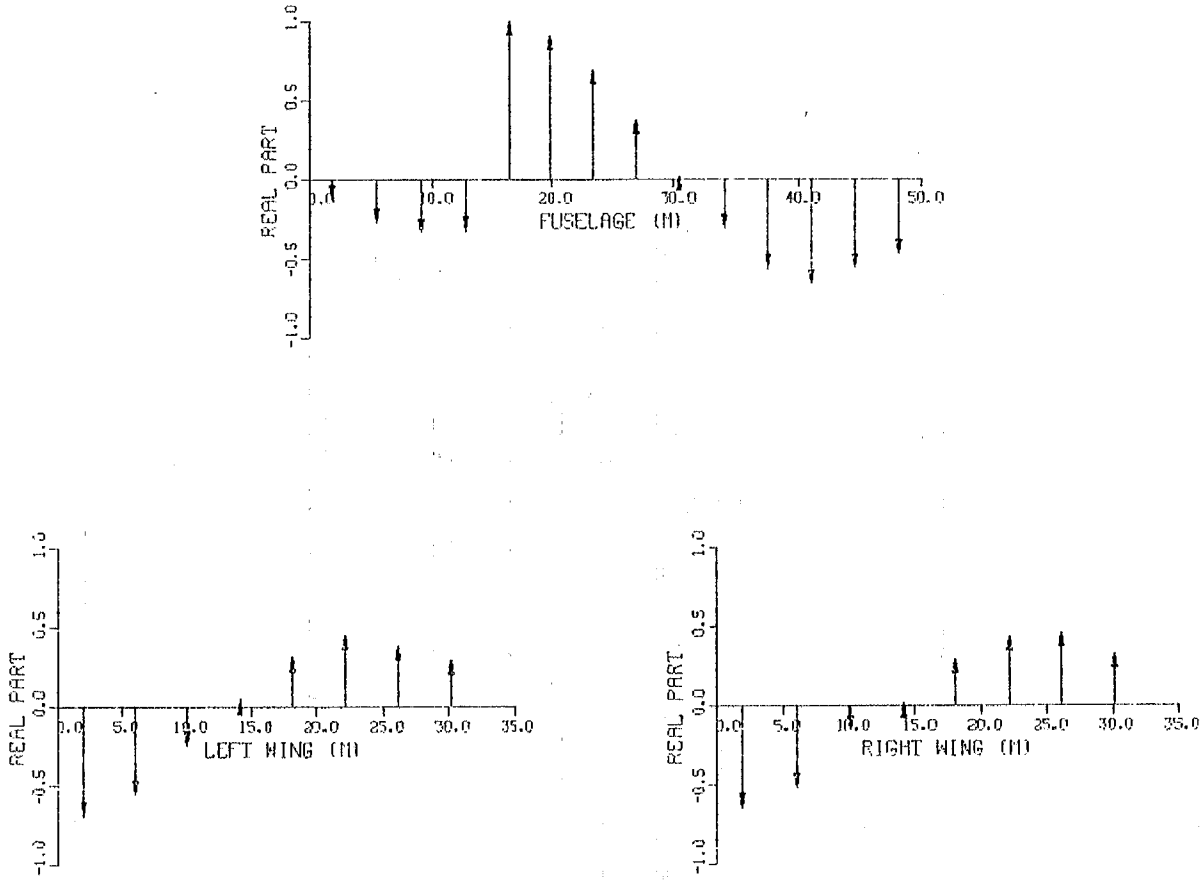

Figure 7. Real part of the fifth normalized natural mode.

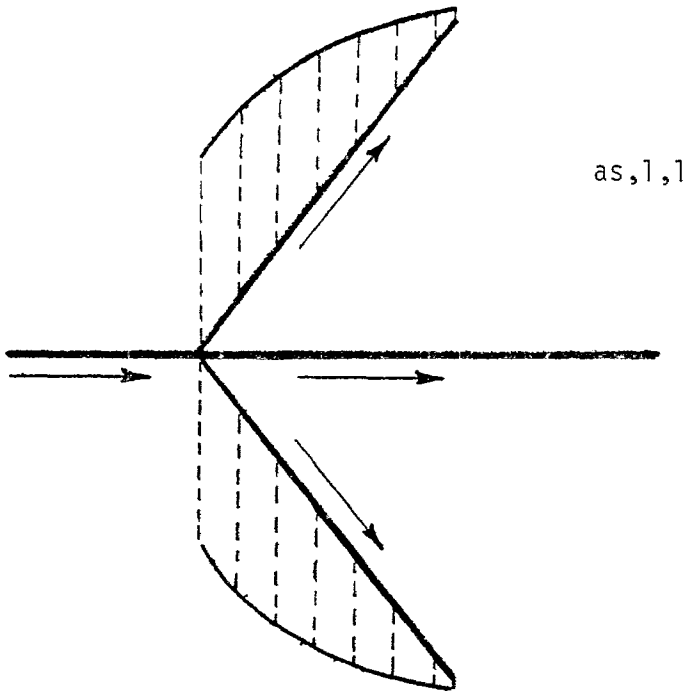

Figure 8. Three-dimensional plot of the real part of the first natural mode.

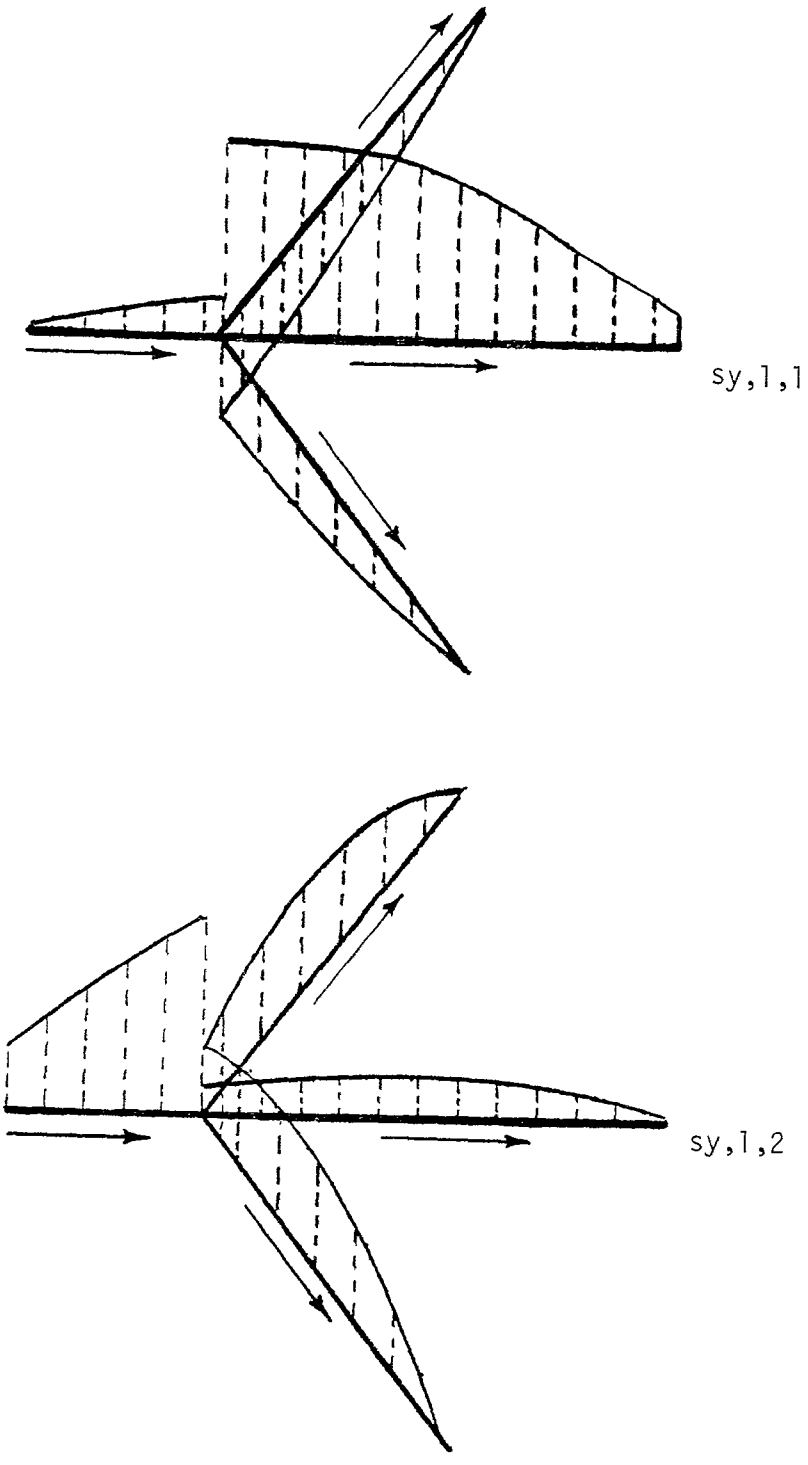

Figure 9. Three-dimensional plot of the real parts of the second and third natural modes.

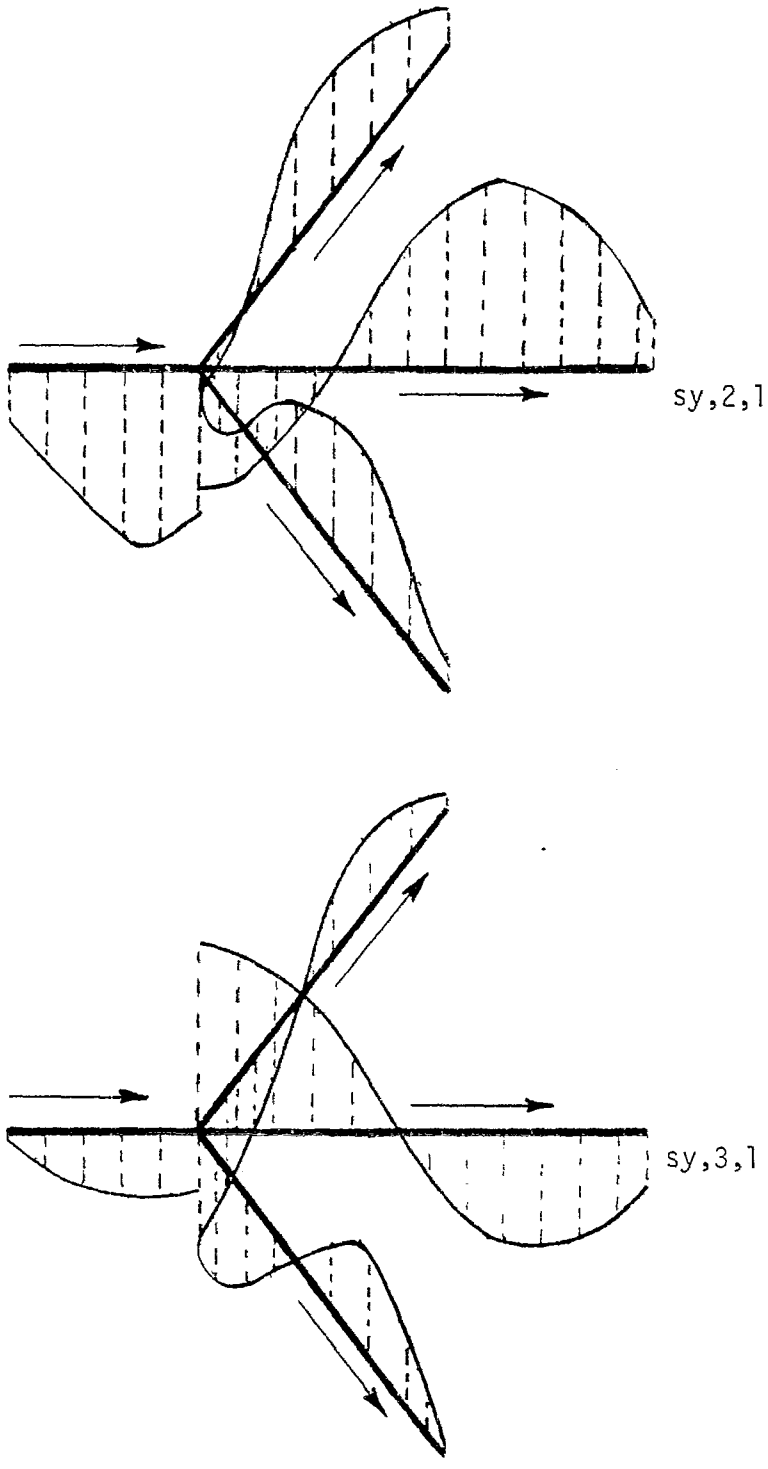

Figure 10. Three-dimensional plot of the real parts of the fourth and fifth natural mode.

3.1.4 The Coupling Coefficients

As can be seen from Equation 2, the α-coupling coefficient contains the variation of the residue as the function of θ and ϕ. For a fixed segment we calculated the residues for several combinations of θ and ϕ. The segment can be chosen from the normalized natural mode plot so that the peak of each mode corresponds to the chosen segment on the scatterer. The normalized variation in these residues gives the $\eta_\alpha^1(\theta,\phi)$.

The normalized coupling coefficients for the five resonances are presented in Figures 11 through 15, with both real and imaginary parts shown. Each curve shows the ϕ variation of residue for a fixed value of θ. Three θ values were chosen, $\theta = 30°$, $\theta = 60°$, and $\theta = 90°$. Due to the symmetry of the wire model, the $\eta_\alpha^1(\theta,\phi)$ is an even function of ϕ, that is, $\eta_\alpha^1(\theta,\phi) = \eta_\alpha^1(\theta,-\phi)$.

It should be noted that the definition of the exciting field orientation (θ and ϕ) is based on the coordinate system and is independent of the location of the wire model. For the same incident field orientation, the induced current response on the scatterer may be different, depending on the location of the wire model in the coordinate system. Hence,the coupling coefficients will be affected, if the location of the wire model is changed. In the foregoing simulation, the wire model was placed so that the fuselage lies on the x-axis with the wing-fuselage junction coinciding with the origin.

It is interesting to know how the coupling coefficients will vary as the wire model is moved along the x-axis. Assume that the wing-fuselage junction is moved from (0,0,0) to (-a,0,0). Then it

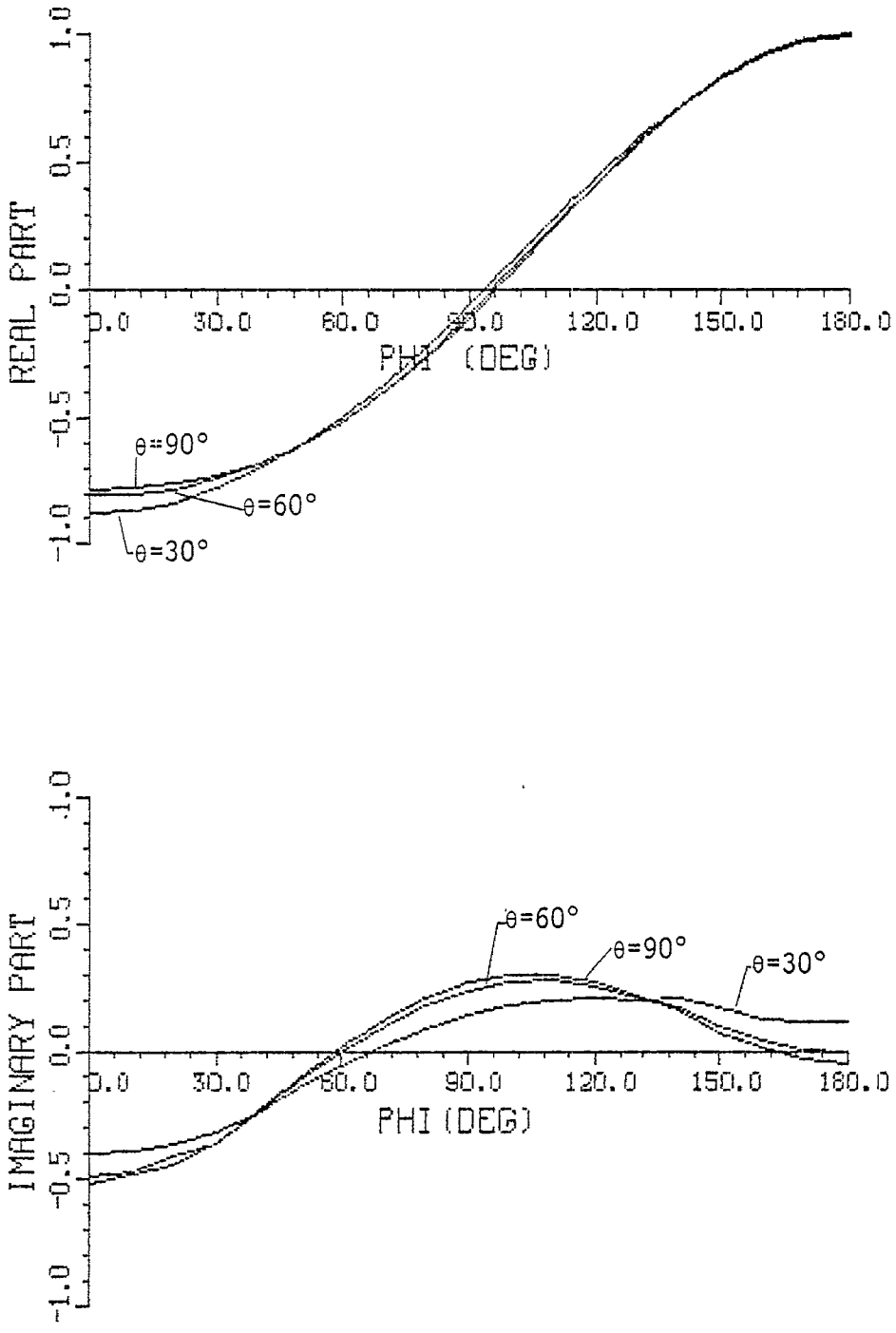

Figure 11. Normalized coupling coefficient of the first natural frequency, as,1,1.

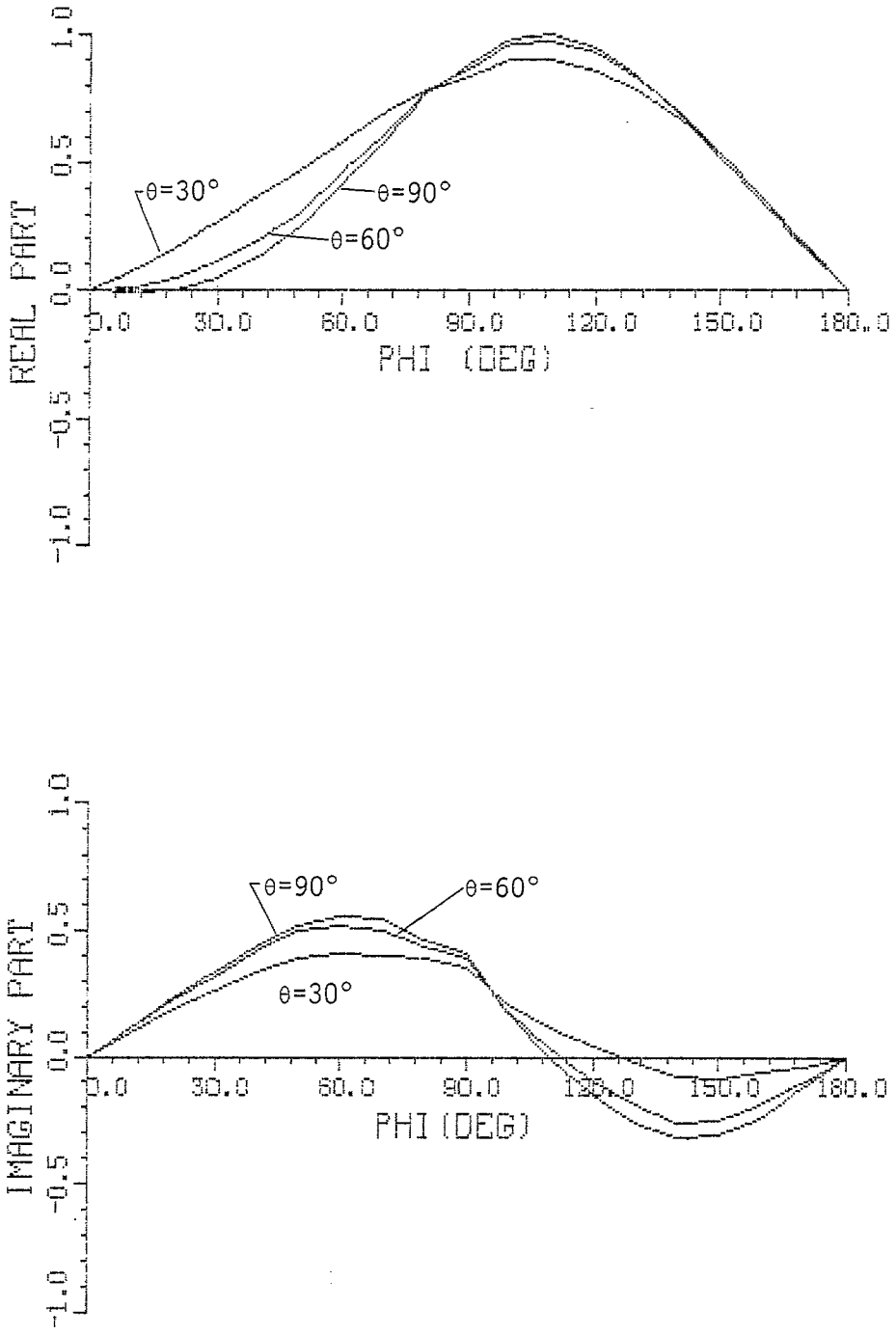

Figure 12. Normalized coupling coefficient of the second natural frequency, sy,1,1.

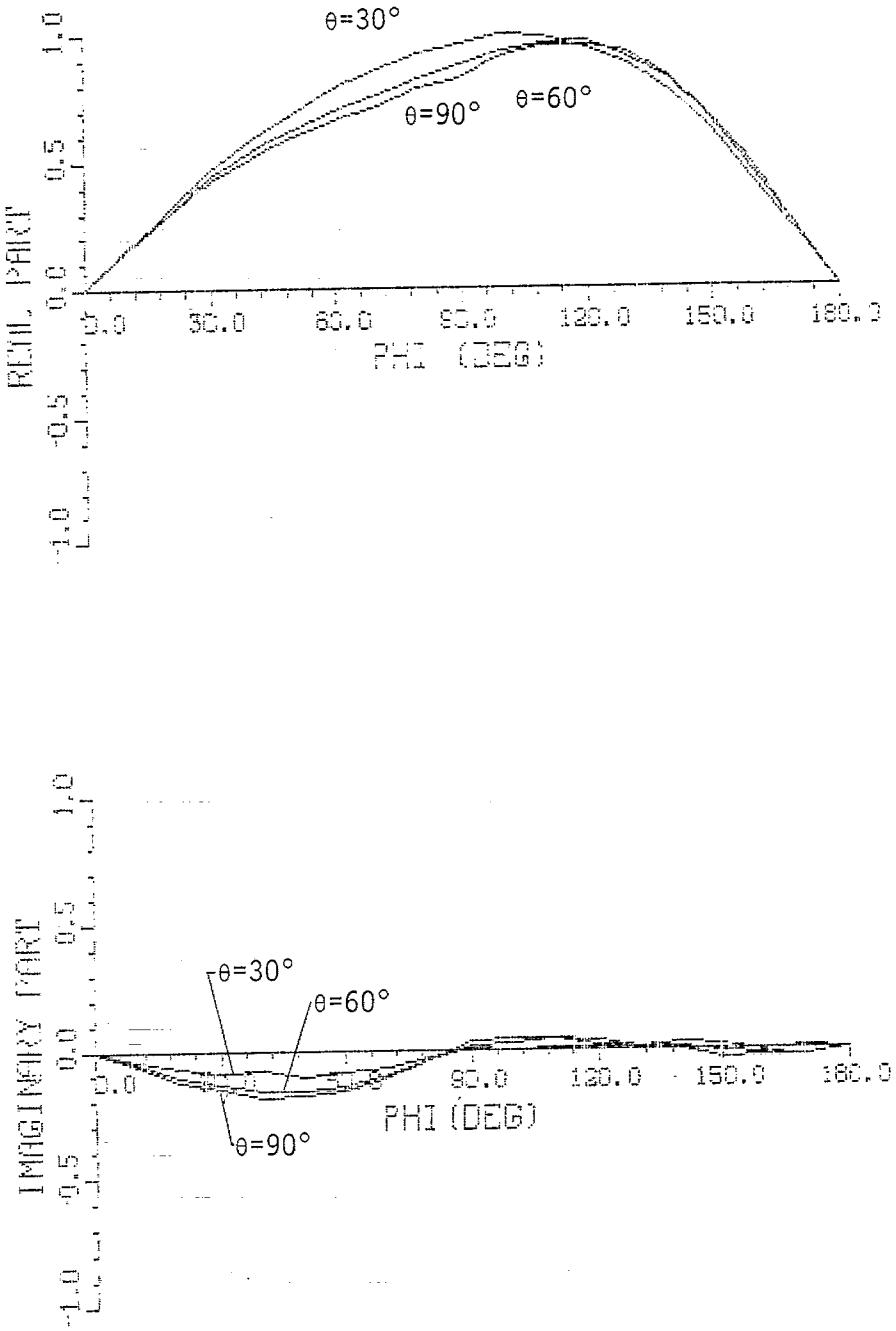

Figure 13. Normalized coupling coefficient of the third natural frequency, sy,1,2.

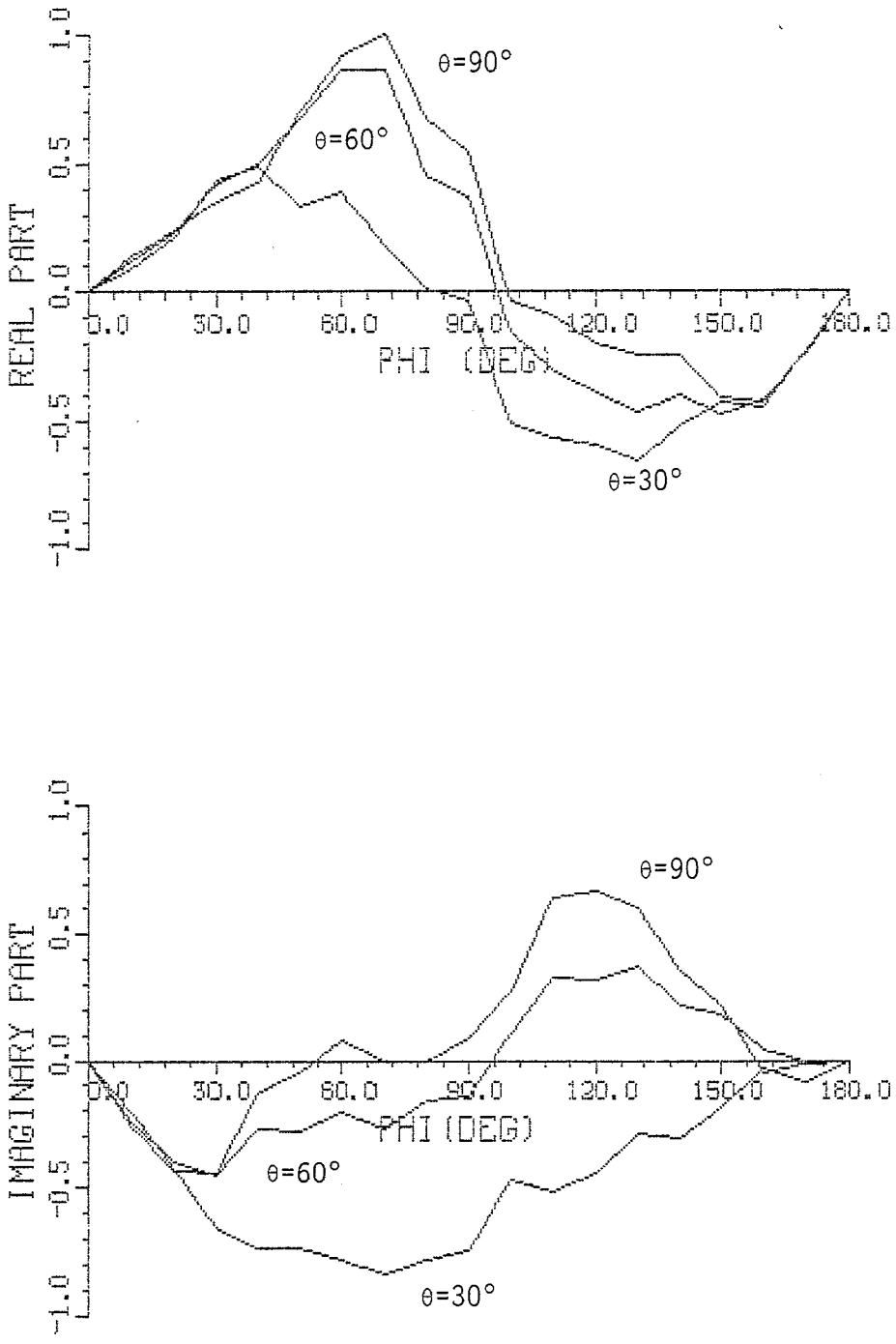

Figure 14. Normalized coupling coefficient of the fourth natural frequency, sy,2,1.

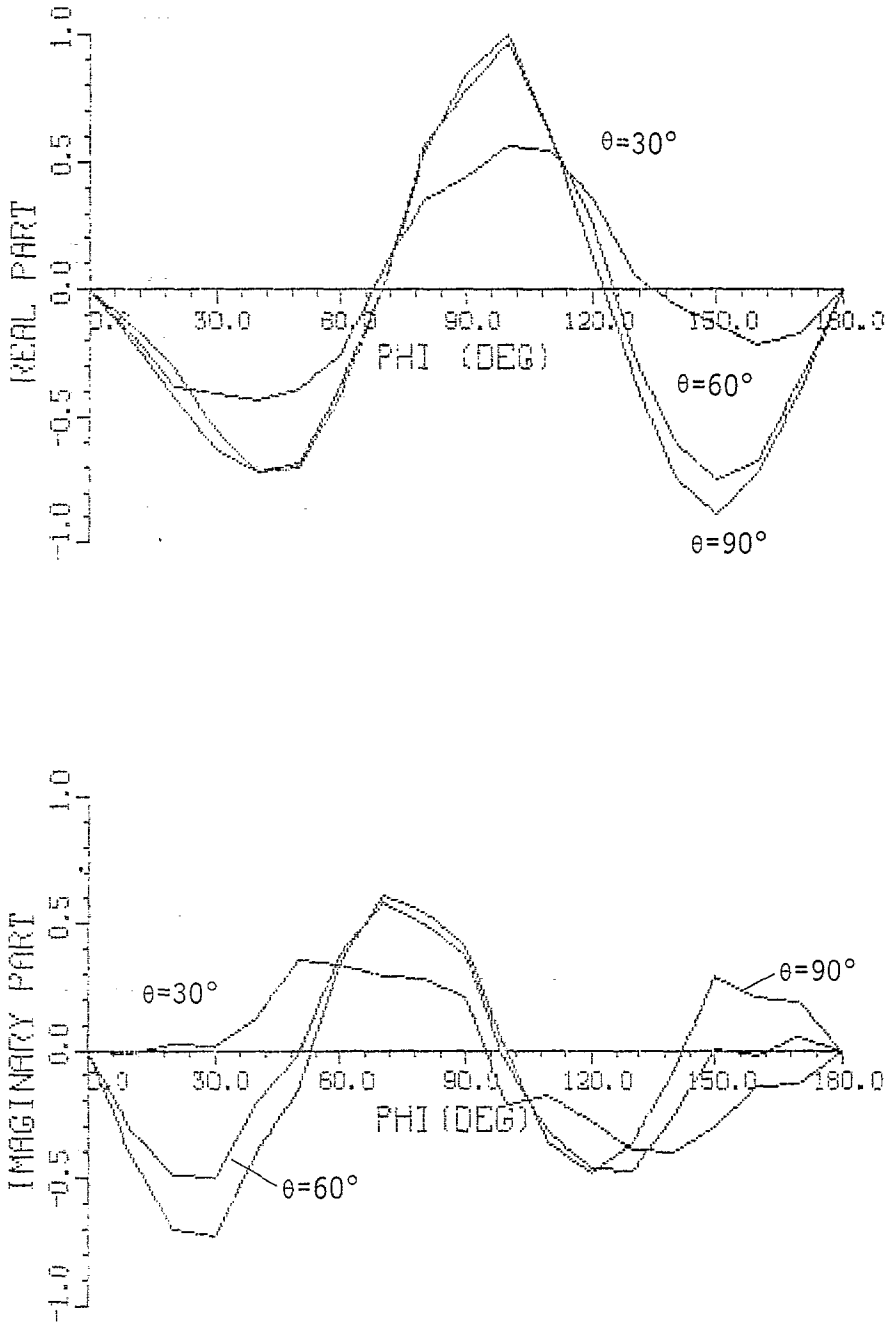

Figure 15. Normalized coupling coefficient of the fifth natural frequency, sy,3,1.

can be argued that for plane wave excitation the coupling coefficients will change as

$$\eta_\alpha^1(\theta,\phi)_{new} = \eta_\alpha^1(\theta,\phi)_{old} \cdot \exp(s_\alpha \cdot a \cdot \cos\phi \cdot \sin\theta / c) \qquad (6)$$

where $\eta_\alpha^1(\theta,\phi)_{old}$ are the coupling coefficients shown in Figures 11 through 15 and $\eta_\alpha^1(\theta,\phi)_{new}$ are the coupling coefficients of the moved wire model.

One special case of interest is the midpoint of the fuselage moved to coincide with the origin of the coordinate system. This puts the origin at the center of the smallest sphere containing the scatterer. Using Equation 6, the new coupling coefficients are computed and shown in Figures 16 through 20.

Figure 21 presents the θ variation of the residues with ϕ chosen to be 90° for all five natural frequencies. Only the real parts are shown, since the imaginary parts are all very small.

3.1.5 The Normalization Factors

The normalization factors can be computed from Equation 4, where $R_\alpha(\theta,\phi,x,y)$ represents the residue obtained from the current response caused by an incident pulse striking the origin at t = 0. In all the preceding graphs, the time origin was chosen so that at t = 0 the incident wavefront was D_o meters from the origin. D_o is chosen for convenience in running the thin wire code. Also, the $R'_\alpha(\theta,\phi,x,y)$ in Equation 4a is obtained not from the transient response starting at t = 0, but from those which start at a later time, $t = t_s$. From Equation 4a, we have

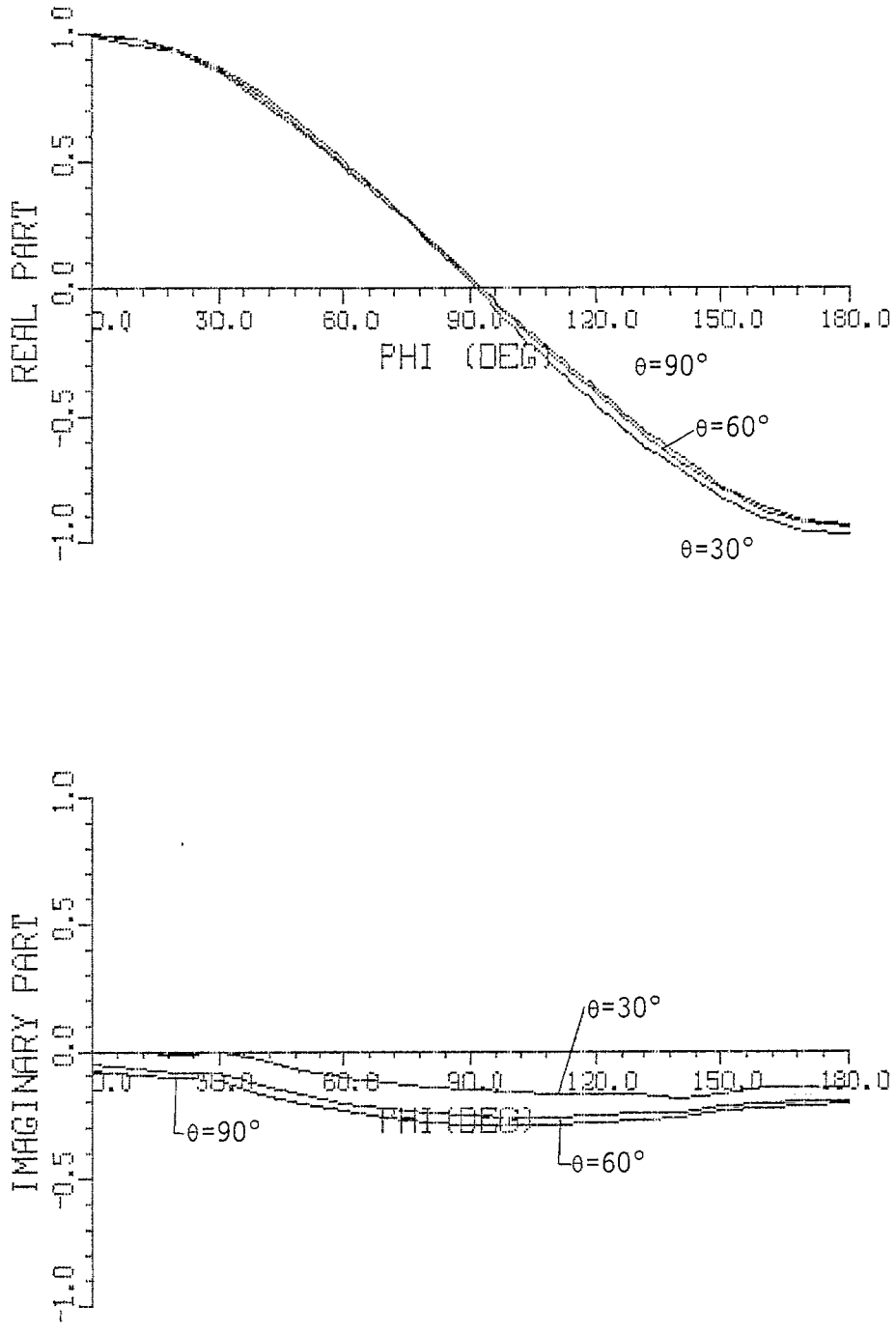

Figure 16. The coupling coefficient of the first natural frequency computed by Equation 6.

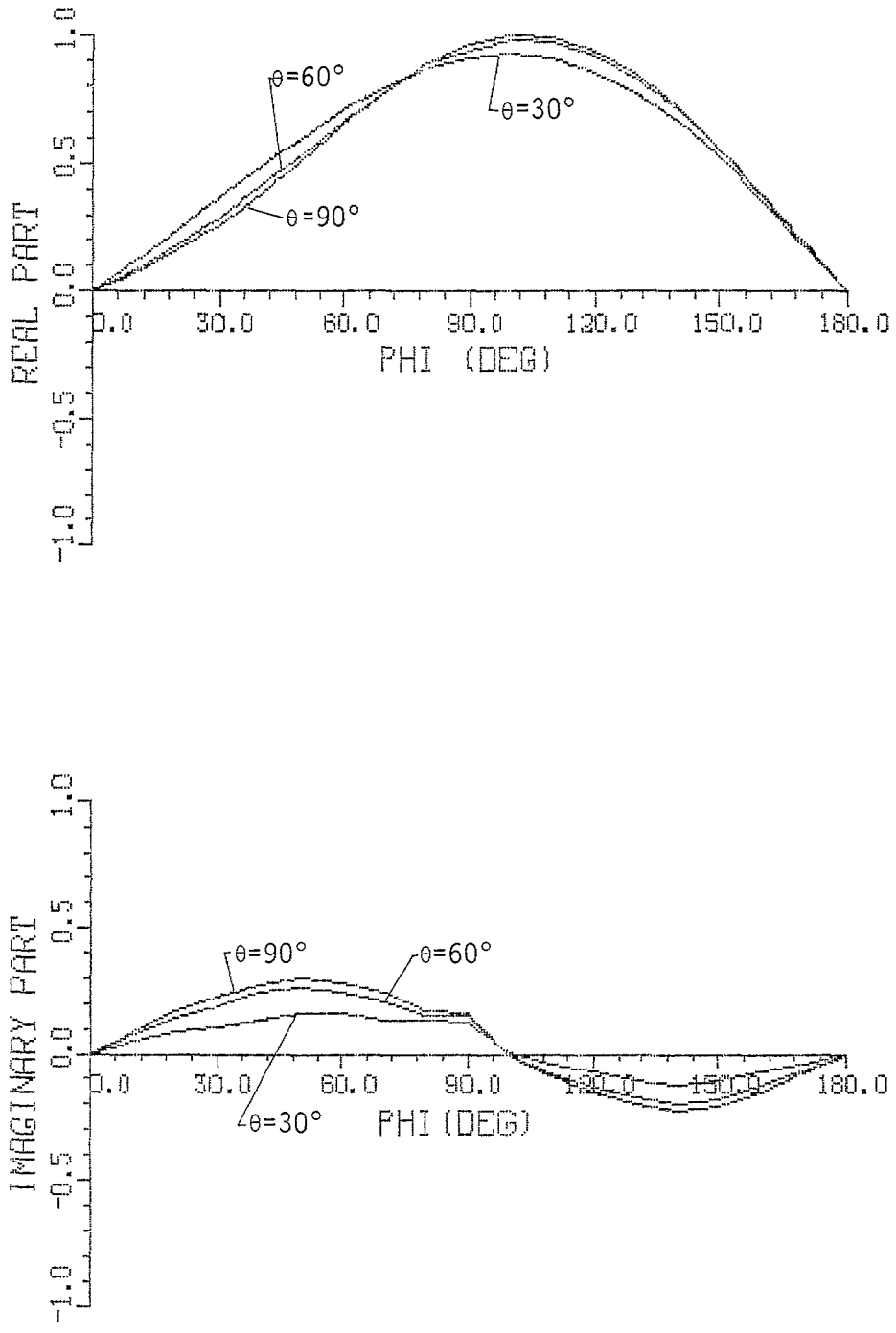

Figure 17. The coupling coefficient of the second natural frequency computed by Equation 6.

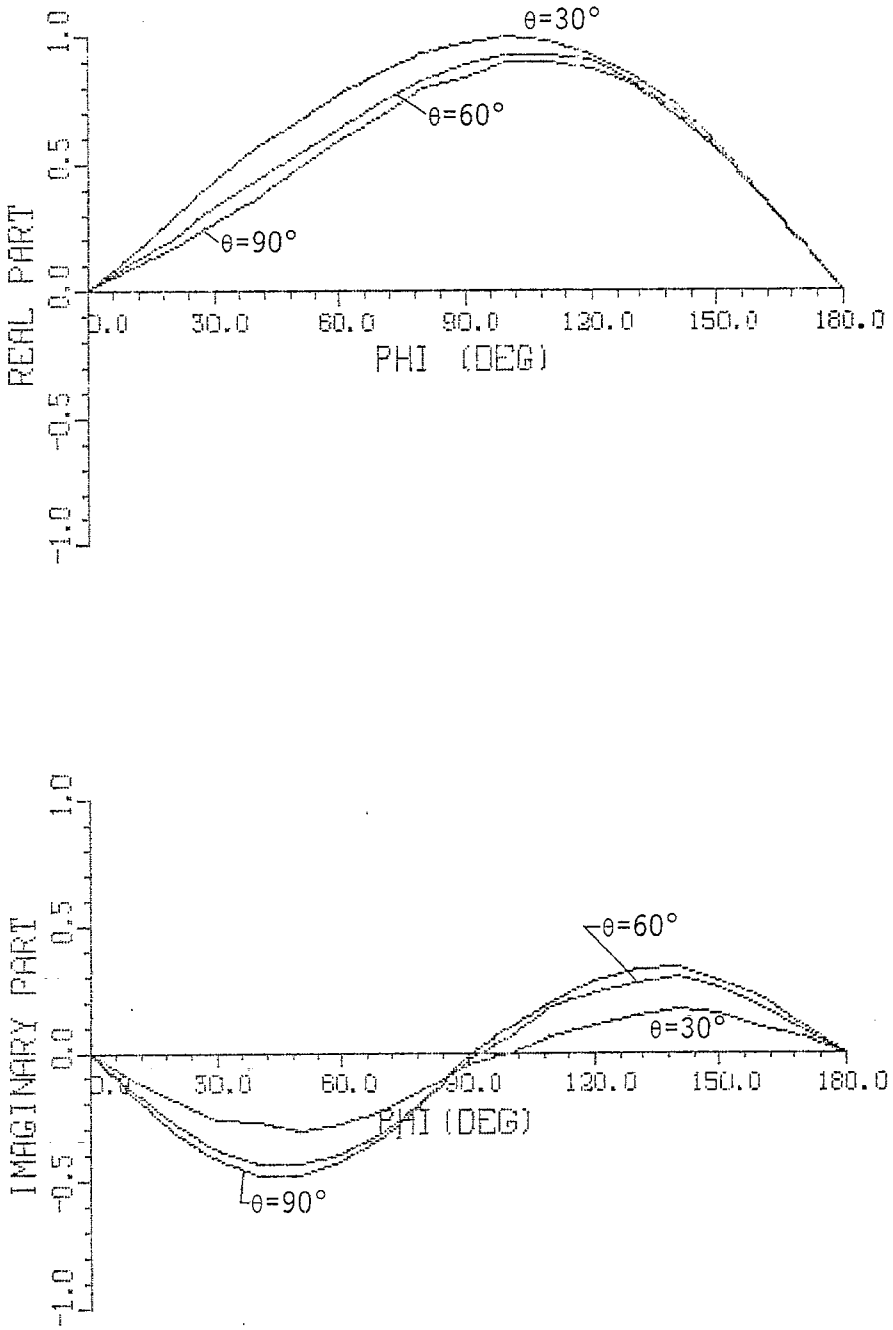

Figure 18. The coupling coefficient of the third natural frequency computed by Equation 6.

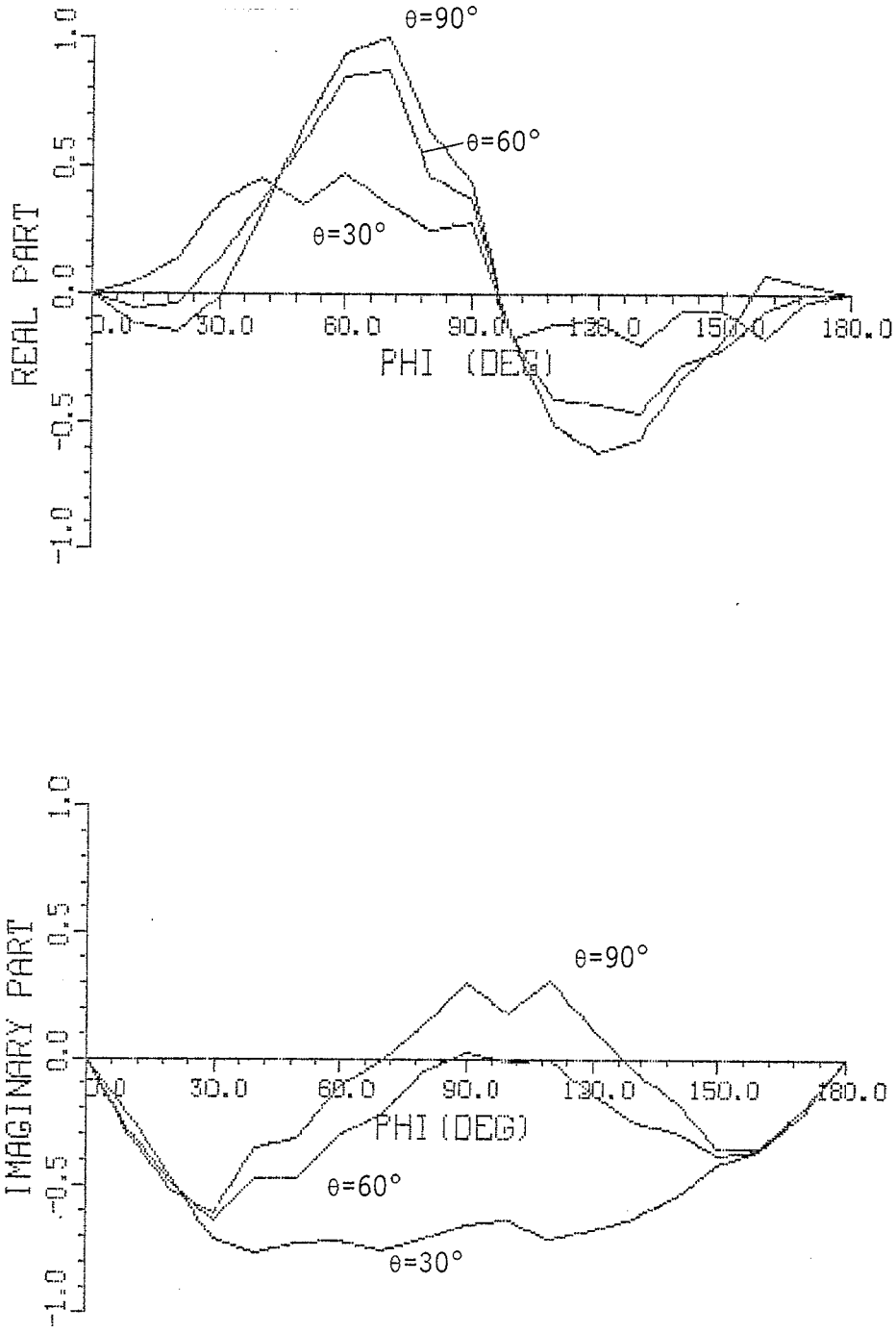

Figure 19. The coupling coefficient of the fourth natural frequency computed by Equation 6.

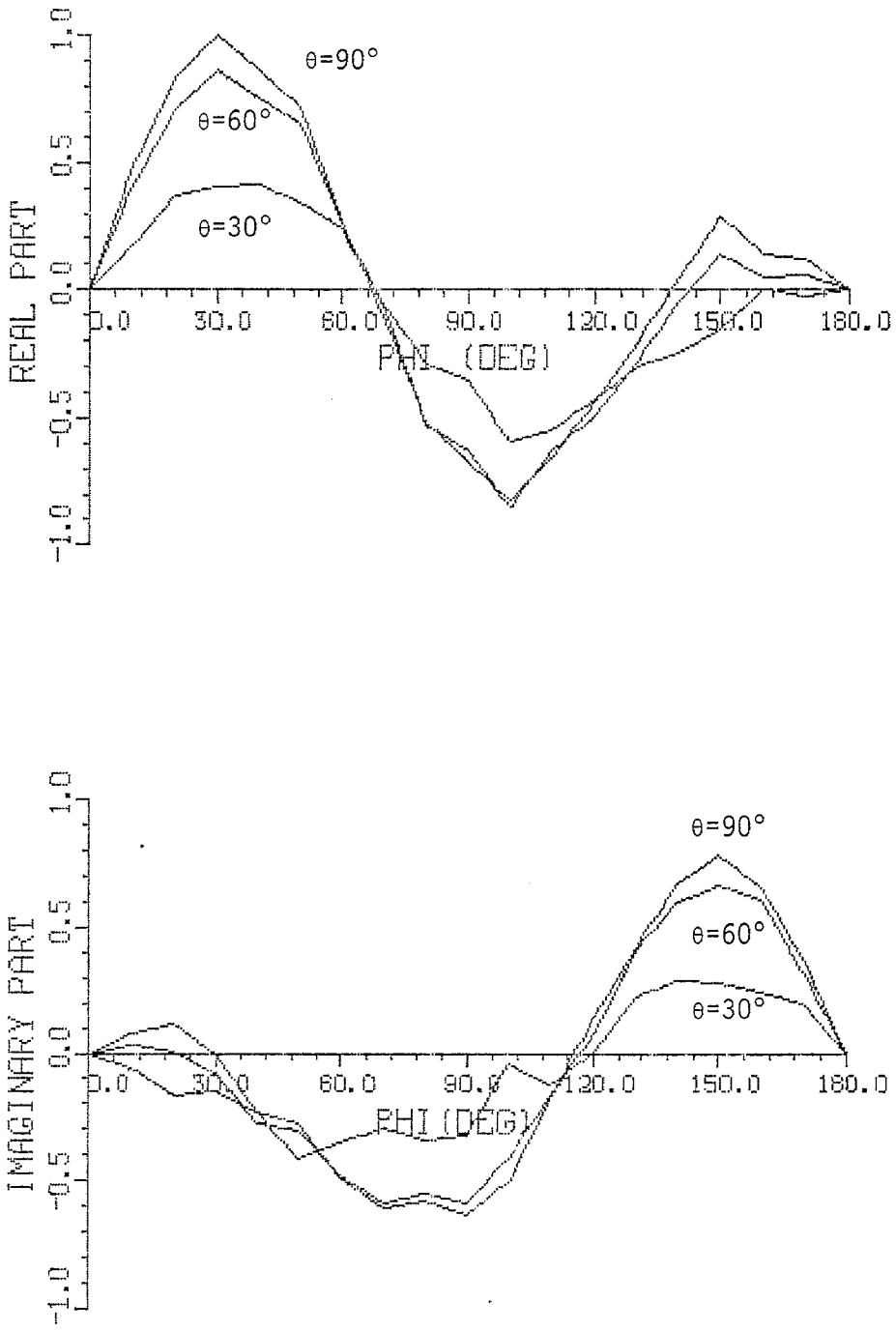

Figure 20. The coupling coefficient of the fifth natural frequency computed by Equation 6.

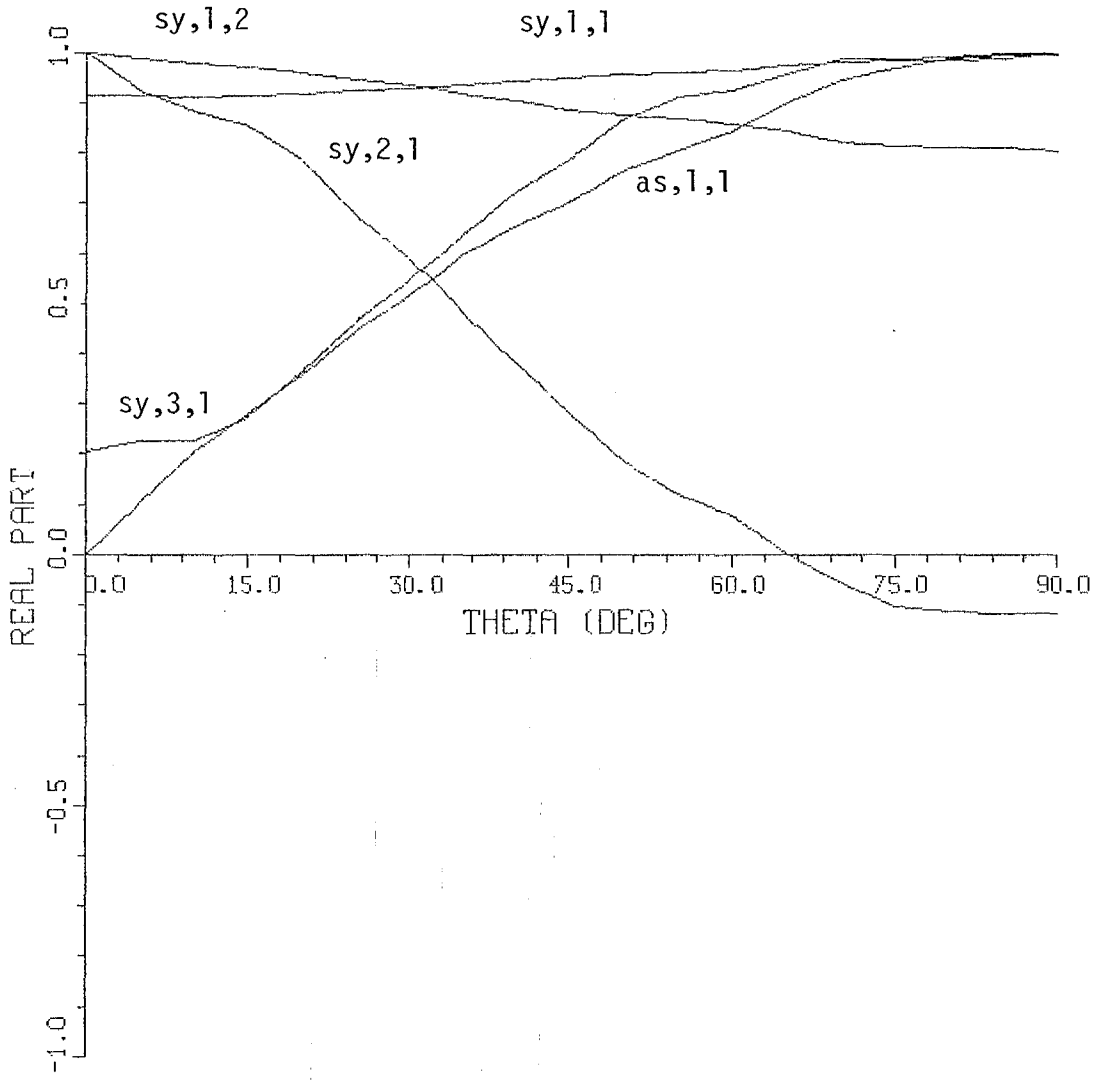

Figure 21. Coupling coefficients, ϕ = 90°.

$$R_\alpha(\theta,\phi,x,y) = R'_\alpha(\theta,\phi,x,y)\exp(-s_\alpha t_1) \qquad (7)$$

The time shift factor $\exp(-s_\alpha t_1)$ in Equation 7 moves the time origin to the time when the incident waveform crosses the origin of the coordinate system, where $t_1 = t_s - D_o/c$.

In this study t_s was chosen to be $t_s = 15\ \Delta t$, and $D_o = 40$ meters. The normalization factors so obtained are

$$\eta_1^{max} = 0.101 \times 10^7 + j\ 0.563 \times 10^5$$

$$\eta_2^{max} = -0.102 \times 10^7 + j\ 0.424 \times 10^6$$

$$\eta_3^{max} = -0.902 \times 10^6 - j\ 0.991 \times 10^6$$

$$\eta_4^{max} = 0.396 \times 10^6 - j\ 0.204 \times 10^6$$

$$\eta_5^{max} = 0.899 \times 10^6 - j\ 0.525 \times 10^5$$

These normalization factors correspond to the coupling coefficients in Figures 16 through 20. The time origin is thus chosen so that at t = 0 the incident wavefront strikes the center of the minimum circumscribing sphere.

3.2 COMPARISON OF THE WIRE MODEL RESULTS WITH OTHER THEORETICAL RESULTS

Taylor et al. [2] found the SEM parameters for perpendicular crossed cylinders in free space. The cylinder lengths and junction point are such that the natural frequencies cannot be compared with our wire model frequencies. However, the natural modes for the two

models are very similar. This indicates that the mode shape is not especially sensitive to the exact model geometry.

The coupling coefficient normalization used in [2] is different from that used here. But the general shape of the coupling coefficients for both models is similar. Some obvious differences exist because of the different geometries. For example, symmetric excitation cannot excite the antisymmetric modes in the perpendicular crossed cylinder model. But with the wire model having swept back wings, the antisymmetric coupling coefficient zero does not occur at exactly $\phi = 90°$ (see Figures 11 and 16). Neglecting differences of this kind, it appears that the coupling coefficients of the first few modes are fairly insensitive to the relative positions of the wing and fuselage.

Another approach for computing the natural frequencies uses the six-length stick model developed by Bedrosian [6]. Liu et al. [15] employed this model in an attempt to find the natural frequencies of a B-52 aircraft. Several sets of stick lengths and length to diameter ratios were tried. The results do not agree well with the wire model frequencies. No antisymmetric mode was found since a symmetric excitation was considered. The stick model has successfully predicted the natural frequencies of other aircraft. It appears to be better suited for modeling aircraft whose wings and fuselage are more nearly perpendicular.

3.3 COMPARISON OF SIMULATION AND EXPERIMENTAL RESULTS

The iterative premultiply method was applied to the measurement

data (Michigan scale model, ATHAMAS I, ATHAMAS II, and ATLAS I). The poles extracted from these noisy measurements were less stable than those from the thin wire code generated data. The poles obtained from different data sources are listed in Table 2. The s-plane plot of poles is shown in Figure 22. Some of the other SEM parameters were computed and compared with the wire model results.

3.3.1 Comparison with Michigan Data

Figures 23 through 26 show a frequency domain comparison of the Michigan scale model data and the wire model results. In the graphs, the Michigan scale model data have been multiplied by the Laplace transform of the double exponential pulse to make it comparable to the wire model result. Figure 23 shows the frequency comparison with data taken at the nose of the aircraft and orientation 1 excitation. In Figure 24, the field excitation is the same as that in Figure 23, but the data were taken at the middle of the aft fuselage. Both graphs match better in the low frequency region. For frequencies beyond 6 MHz significant differences exist. The first and second symmetric mode resonances (sy,1,1, sy,1,2) appear in Figure 23, while only the first one shows up in Figure 24, since the sy,1,2 has insignificant residues on the aft fuselage region. Figures 25 and 26 show the responses at the midpoint of one wing. Figure 25 presents data with orientation 4 excitation, and Figure 26 shows that with orientation 5 excitation. It should be noted that symmetric excitation (orientation 4) causes a resonance peak corresponding to the first symmetric mode (sy,1,1), while antisymmetric excitation (orientation 5) makes the resonance peak corresponding to antisymmetric mode (as,1,1) show up.

Table 2. Natural Frequencies Computed from All Data Sources

α		Thin wire model	Michigan scale model	ATHAMAS I (HPD)	ATHAMAS II (VPD)	ATLAS (Trestle)
1	as,1,1	$-0.145\times10^{7}+j0.135\times10^{8}$	$-0.155\times10^{7}+j0.137\times10^{8}$	$-0.891\times10^{6}+j0.126\times10^{7}$	---	$-0.186\times10^{7}+j0.123\times10^{8}$
2	sy,1,1	$-0.810\times10^{6}+j0.149\times10^{8}$	$-0.767\times10^{6}+j0.143\times10^{8}$	$-0.120\times10^{7}+j0.140\times10^{8}$	$-0.107\times10^{6}+j0.143\times10^{8}$	$-0.260\times10^{7}+j0.140\times10^{8}$
3	sy,1.2	$-0.312\times10^{7}+j0.196\times10^{8}$	$-0.528\times10^{7}+j0.170\times10^{8}$	$-0.118\times10^{7}+j0.175\times10^{8}$	$-0.104\times10^{7}+j0.197\times10^{8}$	$-0.505\times10^{7}+j0.197\times10^{8}$
4	sy,2,1	$-0.389\times10^{7}+j0.373\times10^{8}$	$-0.373\times10^{7}+j0.353\times10^{8}$	$-0.246\times10^{7}+j0.367\times10^{8}$	$-0.754\times10^{6}+j0.374\times10^{8}$	$-0.354\times10^{7}+j0.340\times10^{8}$
5	sy,3,1	$-0.328\times10^{7}+j0.408\times10^{8}$	$-0.260\times10^{7}+j0.503\times10^{8}$	$-0.221\times10^{7}+j0.474\times10^{8}$	---	---

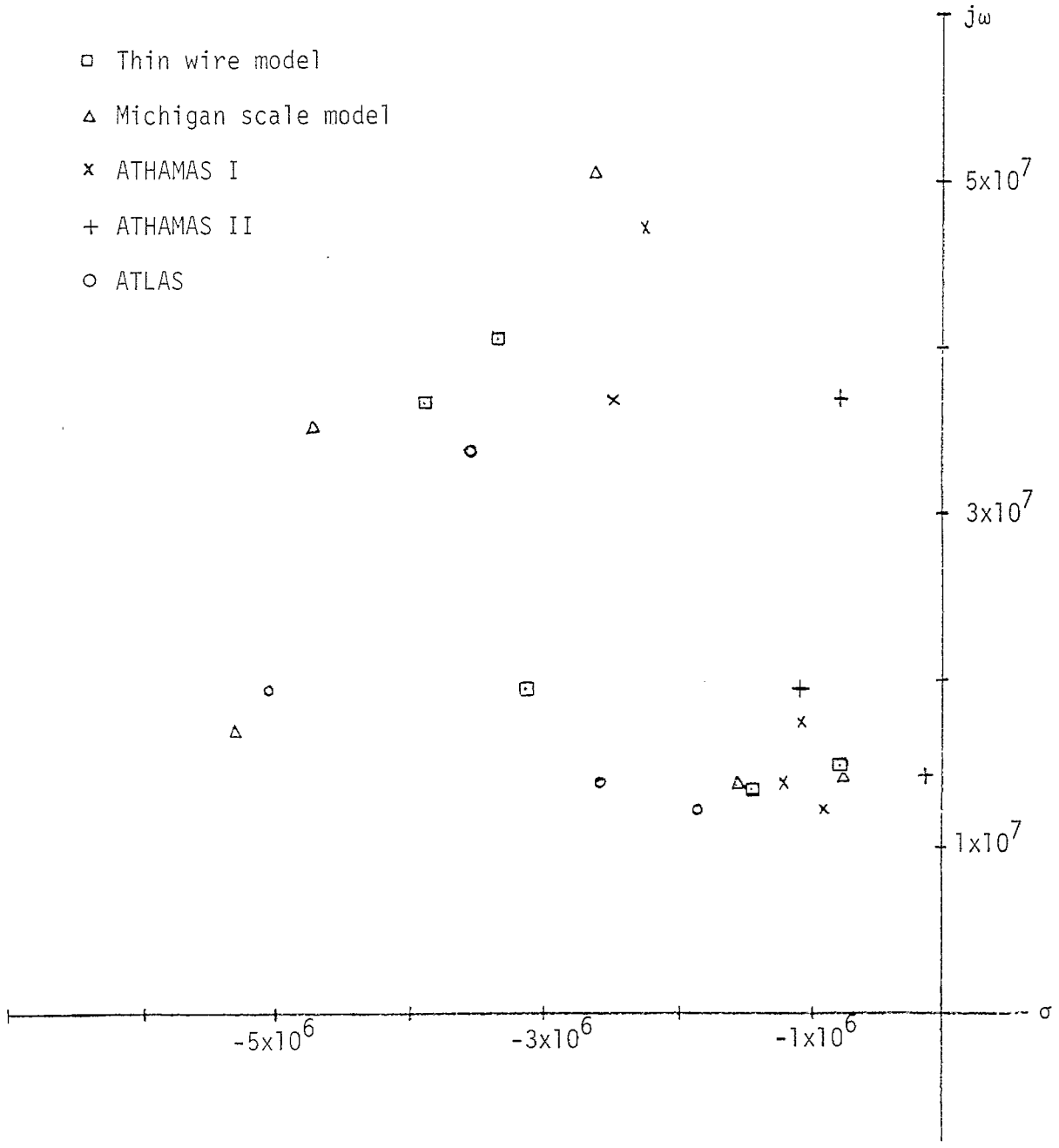

Figure 22. s-plane plot of poles.

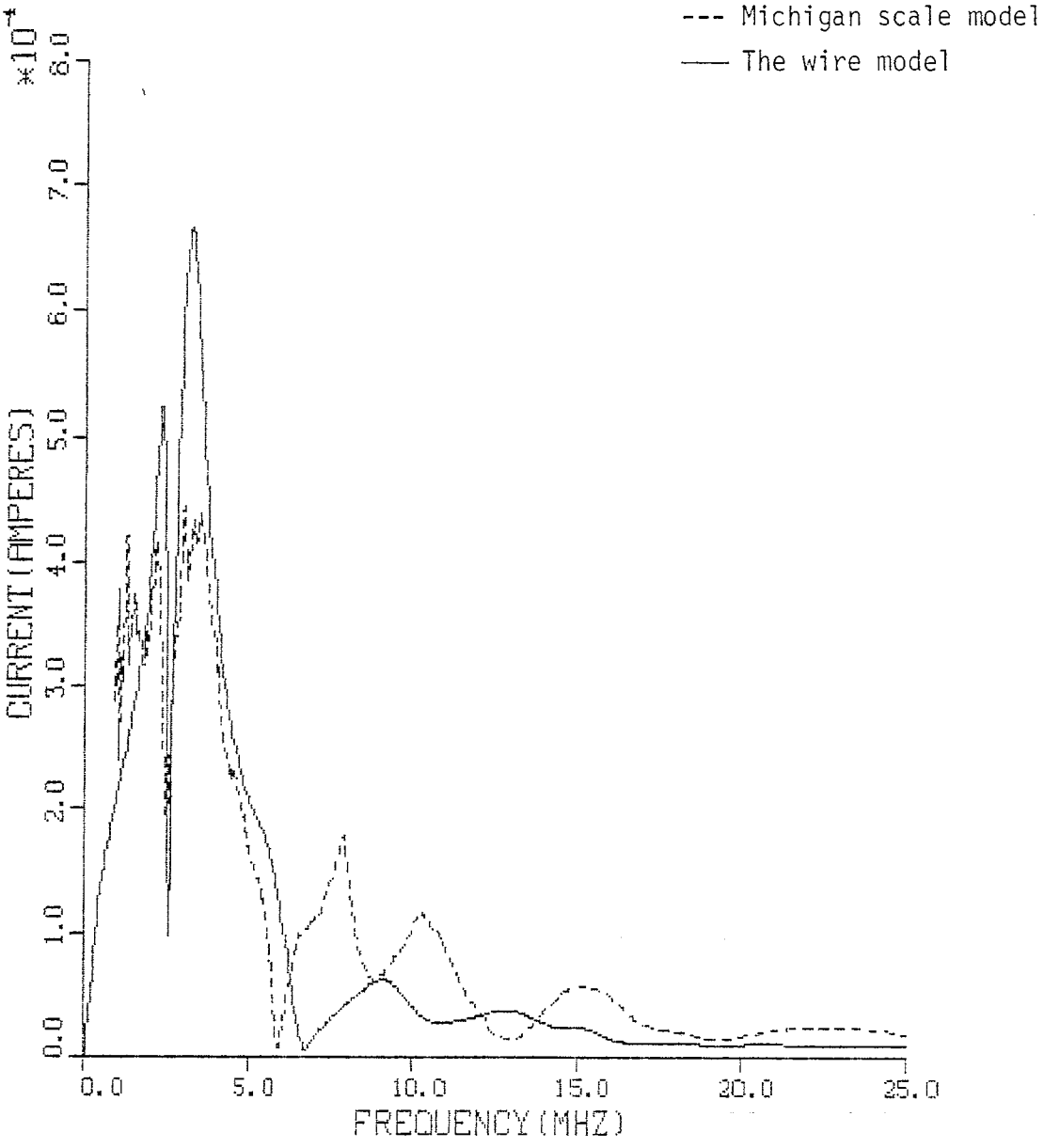

Figure 23. Frequency response comparison at forward fuselage with orientation 1 excitation.

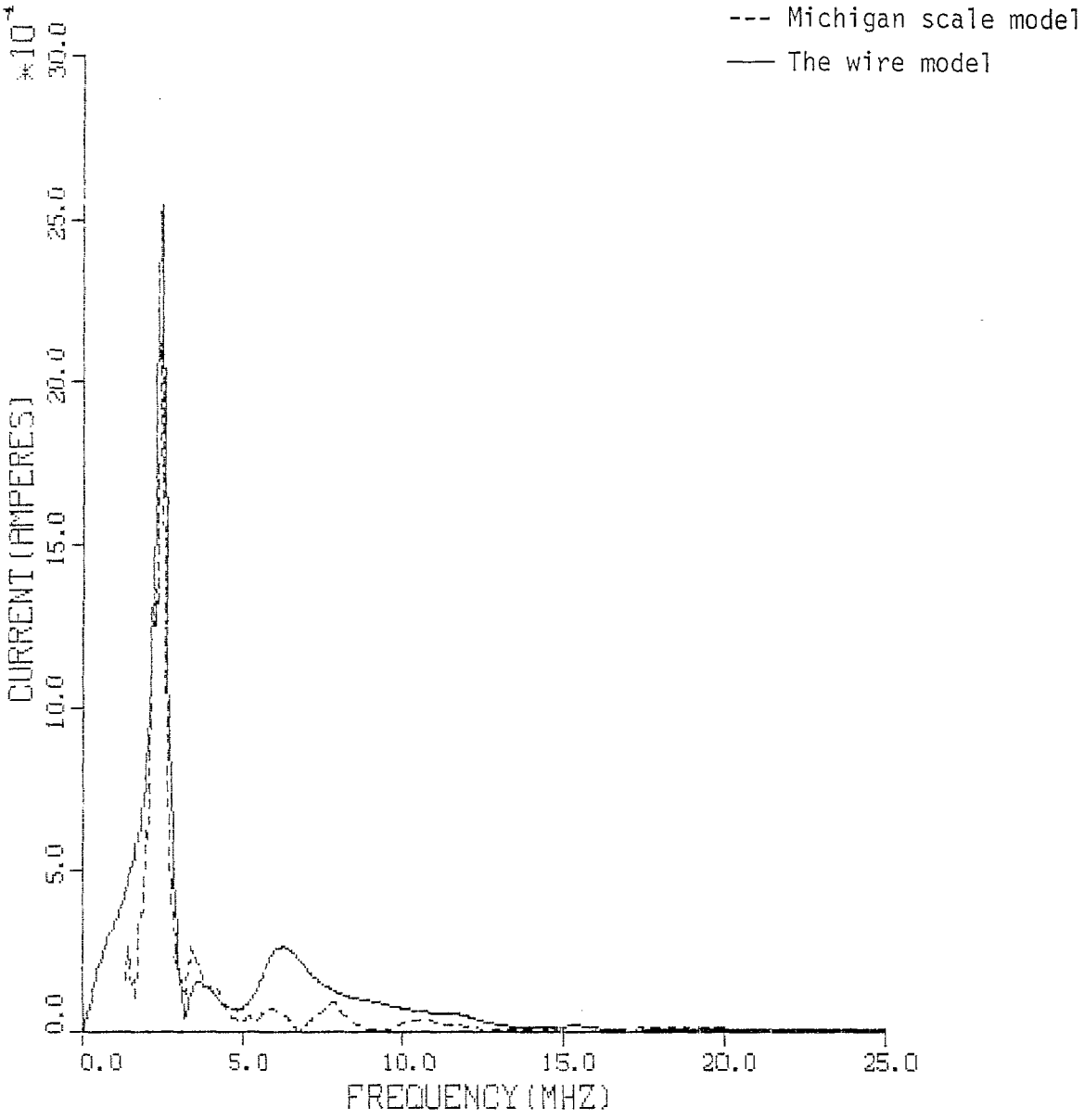

Figure 24. Frequency response comparison at the middle of aft fuselage with orientation 1 excitation.

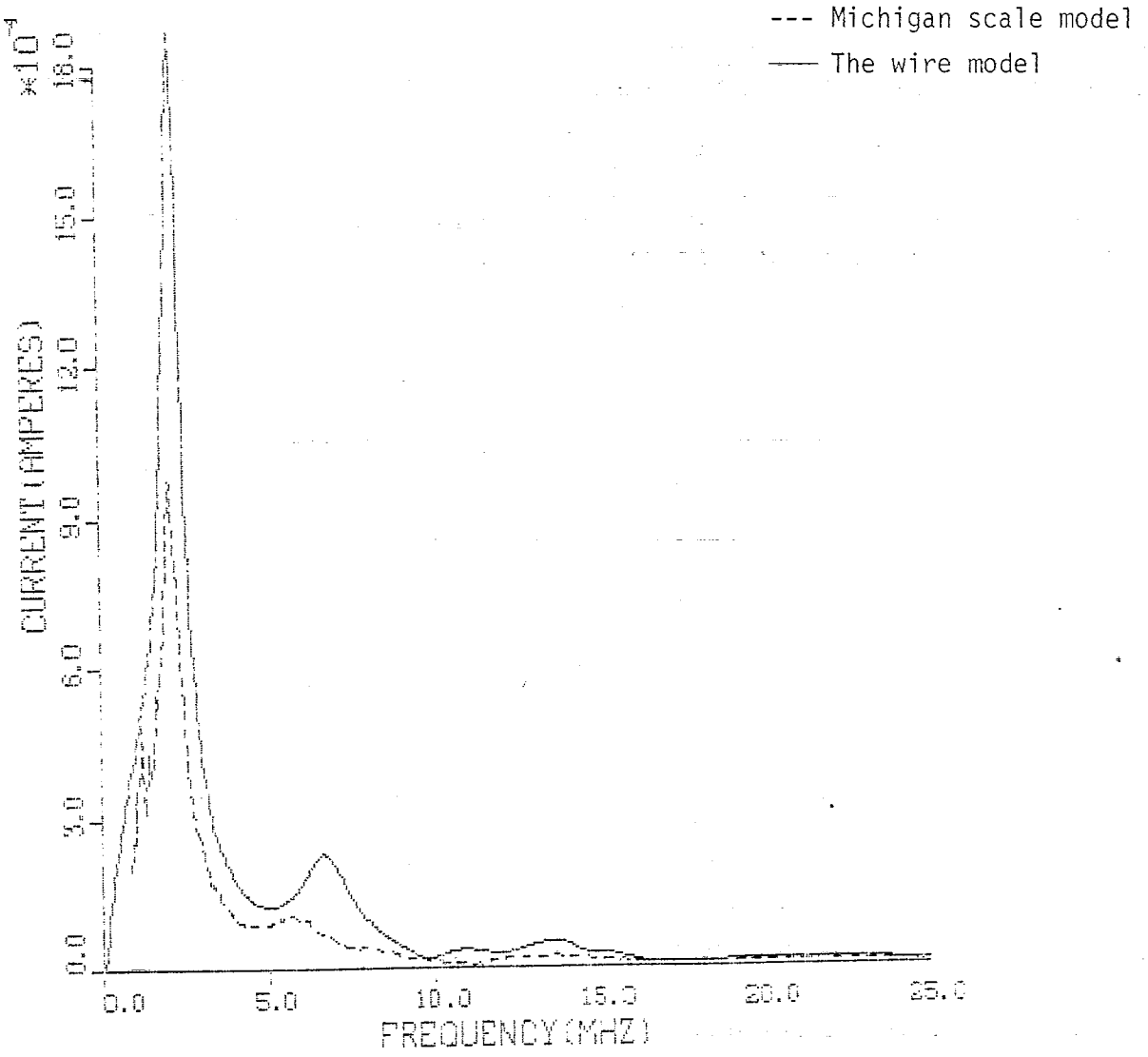

Figure 25. Frequency response comparison at the middle of one wing with orientation 4 excitation.

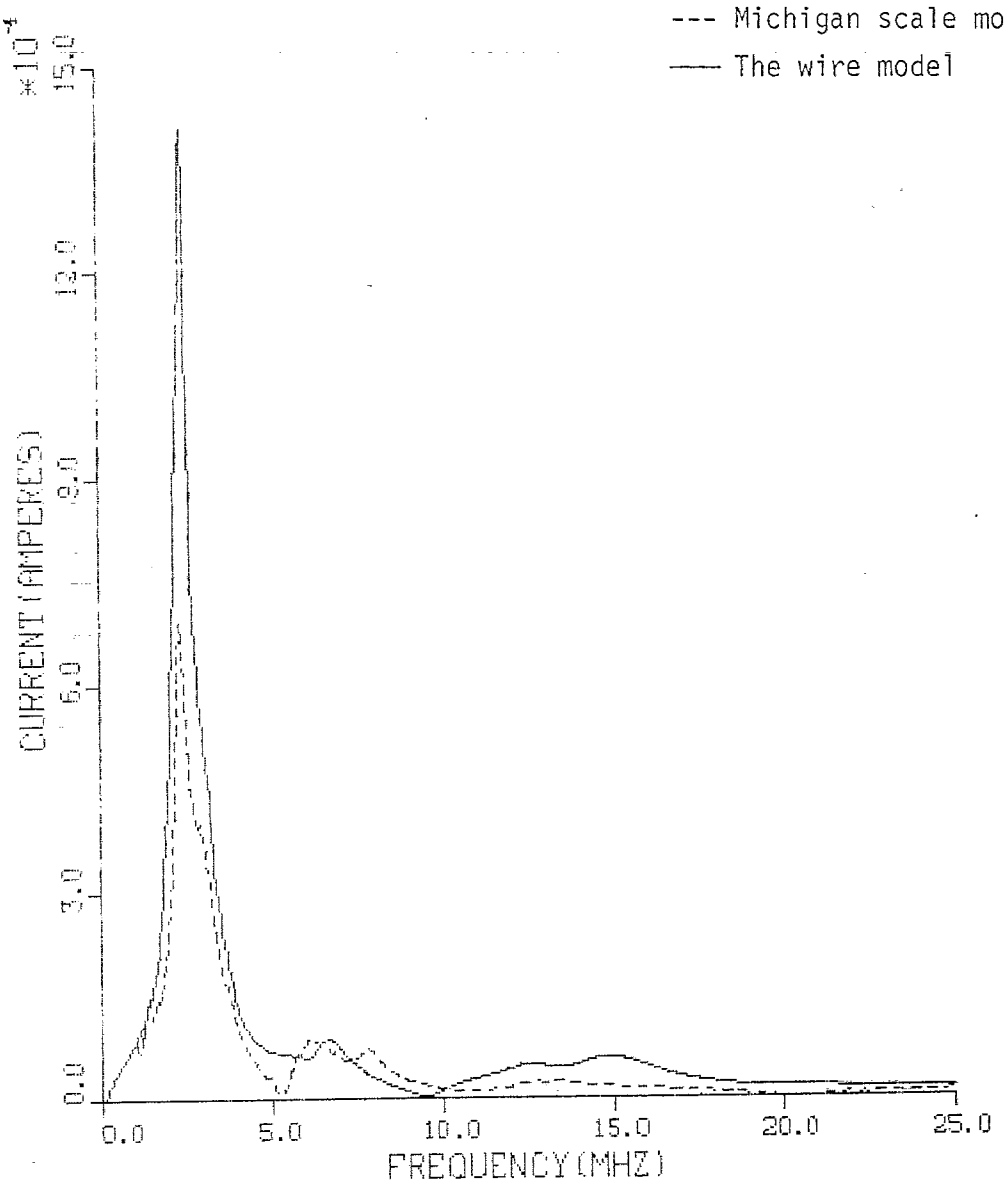

Figure 26. Frequency response comparison at the middle of one wing with orientation 5 excitation.

The natural frequencies of Michigan data listed in Table 2 were obtained from several different locations. The sy,1,1 frequency is the average of five pole values from the aft fuselage. The sy,1,2 frequency appeared only for data taken from the forward fuselage. The sy,2,1 and sy,3,1 frequencies are both averages of two pole values from the fuselage. The as,1,1 frequency was observed only on the wings with orientation 5 excitation. There was no single location on the model where all five natural frequencies appear simultaneously. Only poles with large residues, that is, large natural modes and coupling coefficients, were extractable due to noise. It should be noted that the sy,1,1 and as,1,1 frequencies match the wire model values well. The remaining natural frequencies do not agree as well. This is probably due to model error. For example, the wire model omits the tail section and of course does not have a variable radius like the scale model. Data from the "large" scale model was also analyzed, but the results were not consistent and hence, not reported here.

The normalized sy,1,1 natural mode was computed from the Michigan data. The largest sy,1,1 residue from the scale model data was normalized to be equal to the sy,1,1 natural mode from the wire model at the closest location. The remaining residues were normalized with the same factor. The result is compared to the wire model result in Figure 27. The two graphs are very similar along the fuselage. As can be seen from the graph, the data measured on the scale model are not exactly at the same locations as those generated by the thin wire code. This may be one reason for the numerical differences. And the

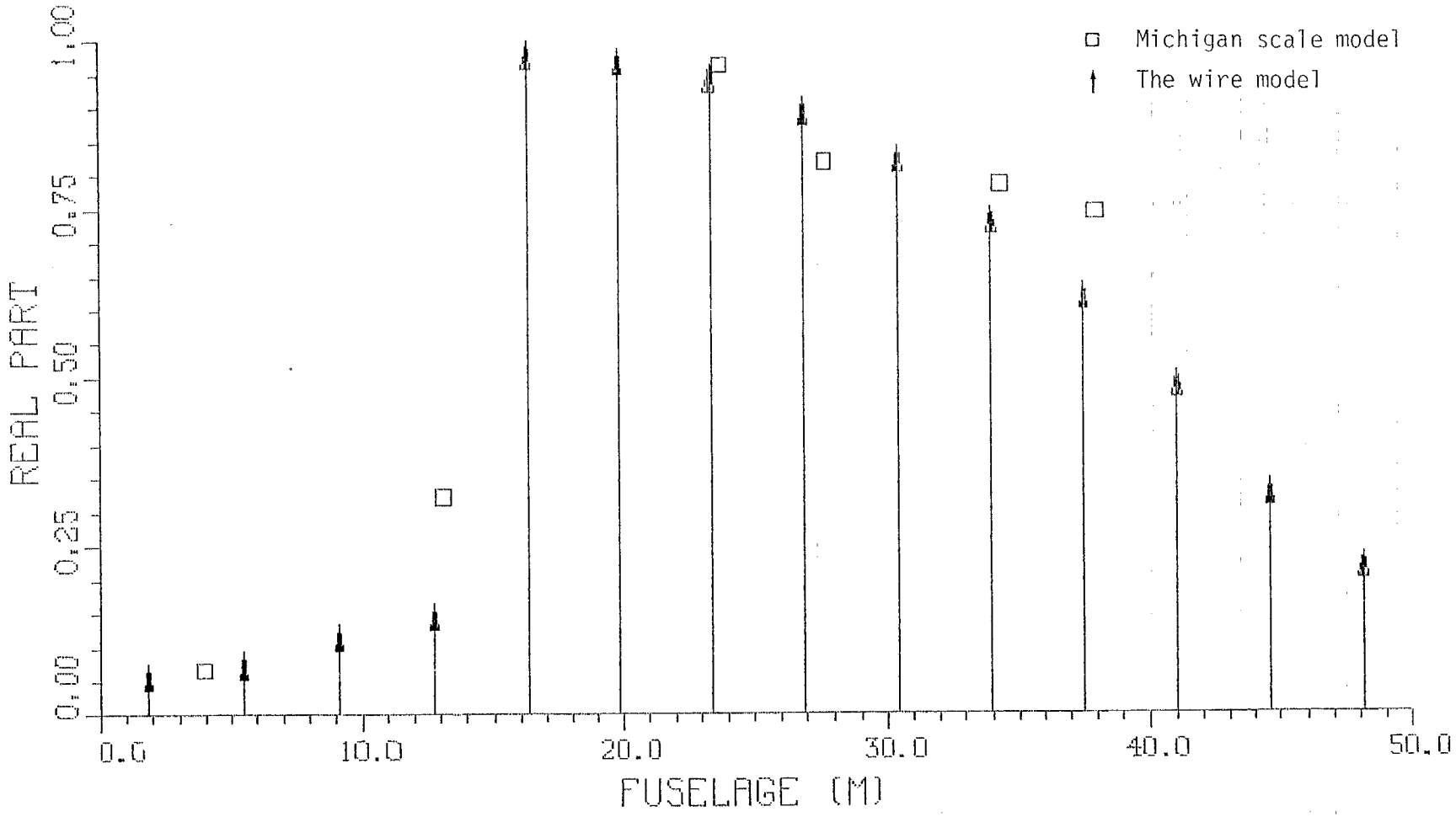

Figure 27. Natural mode comparison: Michigan scale model measurement and the wire model simulation, for sy,1,1.

significant difference in the magnitude of data points close to the tail is probably due to neglecting the tail in the wire model simulation.

Figure 28 shows the sy,1,1 coupling coefficient θ-variation comparison between the Michigan scale model measurement and the wire model simulation. The angle ϕ is 90° in both cases. θ = 0° is orientation 1 and θ = 90° is orientation 4 in the measurement. These were the only two angles of incidence available for this comparison. Figure 29 presents the comparison of ϕ-variation. The angle θ is 90° in both cases, ϕ = 90° is orientation 4 and ϕ = 180° is orientation 5 excitation. The same comparison as in Figure 29 for as,1,1 is shown in Figure 30.

The normalization factors were also calculated from the Michigan data for sy,1,1 and as,1,1. The results are compared to the results from the wire model simulation in Table 3. These results are consistent with the larger peaks observed in the wire model frequency domain data presented above.

3.3.2 Simulator Results

Both the thin wire and Michigan data attempt to model the external coupling problem in a free space, plane wave excitation environment. The simulators (ATHAMAS I, ATHAMAS II, and ATLAS I) do not provide this environment. There is a lossy ground plane in ATHAMAS I and a better conducting ground plane in ATHAMAS II. In ATLAS I an interaction between the simulator structure and test object exists. None of the simulators produces an exact plane wave,

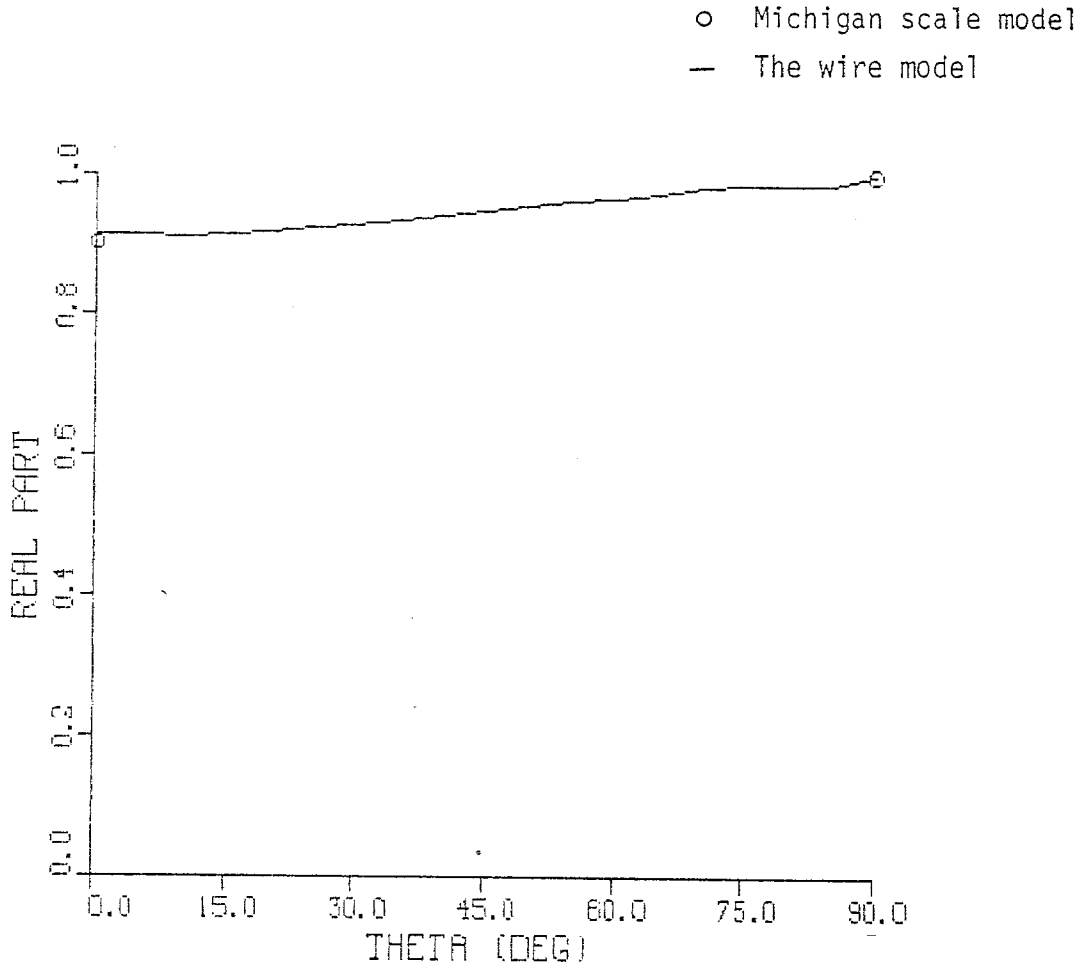

Figure 28. Coupling coefficient for the sy,1,1 natural frequency at ϕ = 90°: Michigan scale model and the wire model simulation.

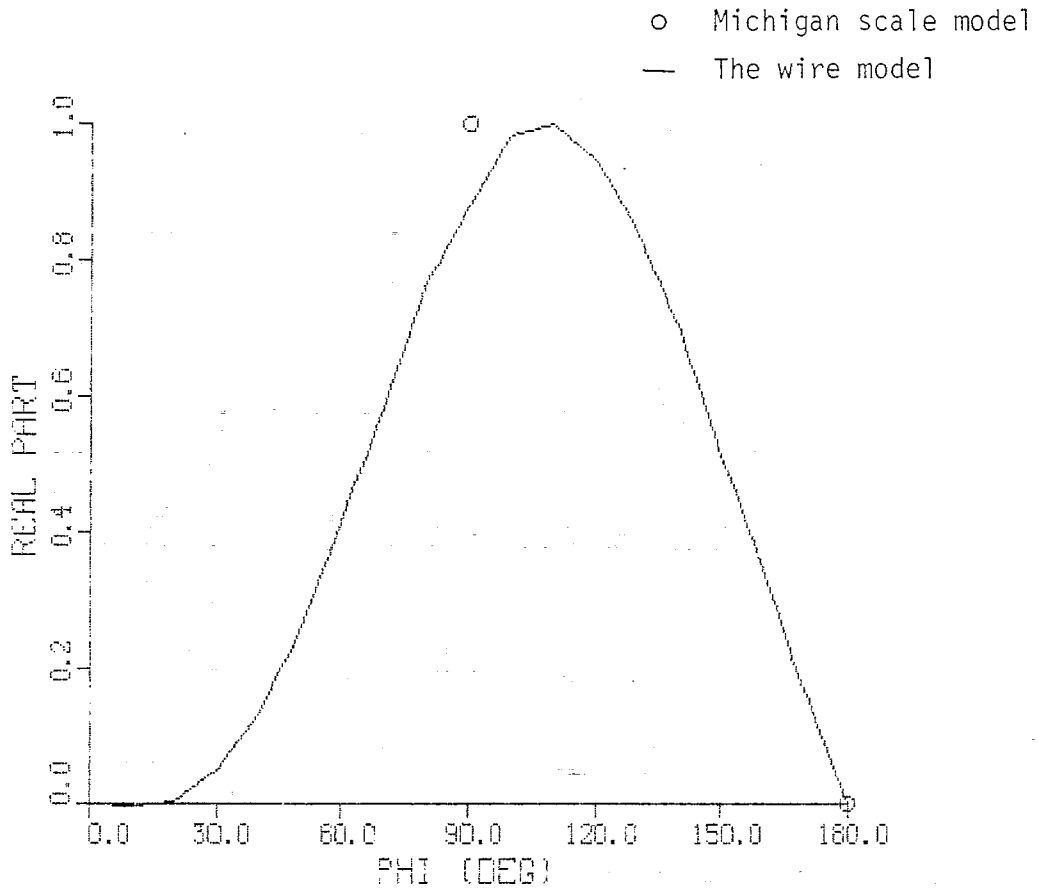

Figure 29. Coupling coefficient for the sy,1,1 natural frequency at θ=90°: Michigan scale model and the wire model simulation.

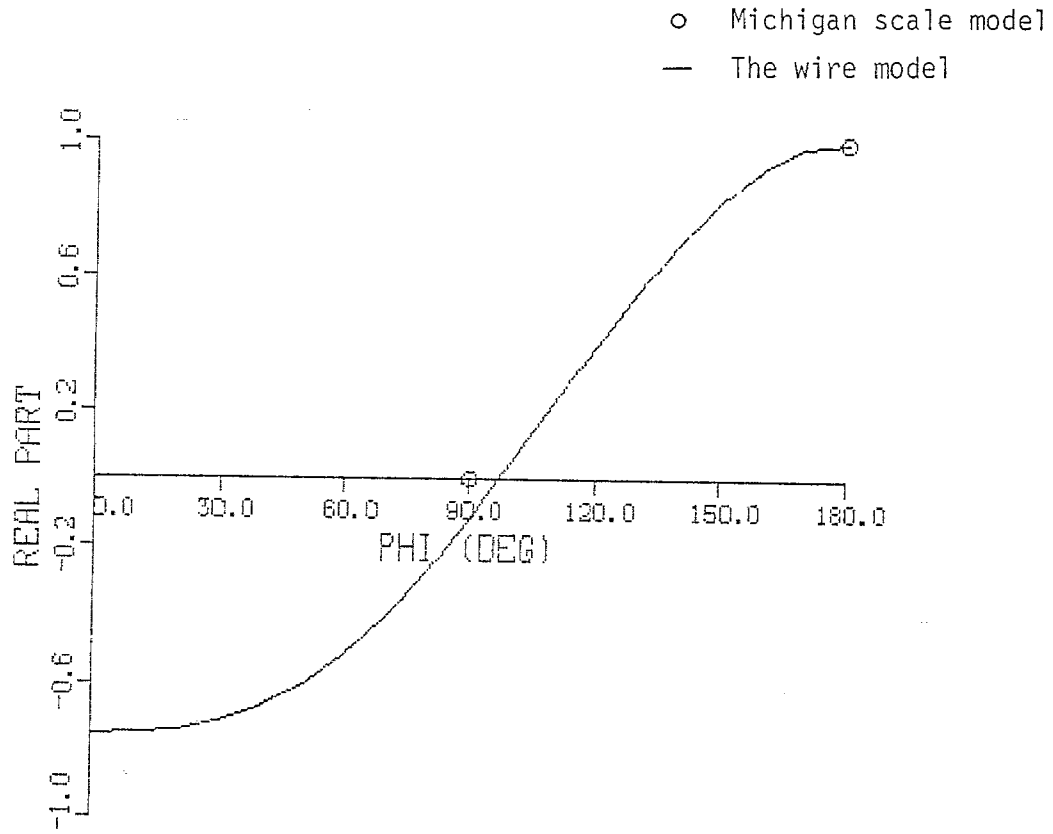

Figure 30. Coupling coefficient for the as,1,1 natural frequency at θ=90°: Michigan scale model measurement and the wire model simulation.

Table 3. Normalization factor comparison

	Thin wire model	Michigan scale model
η_1^{max} (as,1,1)	$0.101 \times 10^7 + j\ 0.563 \times 10^5$	$0.629 \times 10^6 + j\ 0.192 \times 10^6$
η_2^{max} (sy,1,1)	$-0.102 \times 10^7 + j\ 0.423 \times 10^6$	$-0.882 \times 10^6 + j\ 0.651 \times 10^6$

but ATHAMAS II and ATLAS I provide a moderate approximation to a plane wave environment. Some theoretical studies have been made on the effects of these extra interactions. Shumpert [16] computed the SEM parameters for a wire scatterer parallel to a lossy ground. He found that the natural modes are not affected much by the ground plane. But the natural frequencies are sensitive to the conductivity and permittivity of the ground and also to the wire height above the ground. Taylor et al. [4],[5] investigated ground plane effect on the SEM parameters for crossed wire configurations. They concluded that the real parts of the natural frequencies decrease as the wire configuration approaches a perfect conducting ground plane. They also found that a lossy ground plane makes the real parts of the natural frequencies more negative compared with the free space case. Lam [17] studied the interaction between a parallel plate simulator and a

cylinder. They found that the dependence of pole location on the distance between the test object and simulator is oscillatory.

The natural frequencies calculated from the ATHAMAS I data are listed in Table 2. As in the Michigan scale model case, the various poles appear at different aircraft locations. No current waveform at a single location contains all the natural frequencies listed. The antisymmetric mode appears only on the wings as expected. There are variations in the value of the same pole as the test location is changed. Poles from different measurement locations were averaged to give the final values. From the results in [5], the lossy ground plane should make the pole real parts more negative. However, we can see from Table 2 that only the sy,1,1 mode follows this trend. The difference may be due to measurement error. No attempt was made to compute natural modes or coupling coefficients since not enough measurements were available. Overall, the data from ATHAMAS I yielded poorer results than that from the other simulators.

Only one measurement was available from the ATHAMAS II simulator. It was taken on the fuselage with a vertical incident electric field orientation not considered in the wire model. Three natural frequencies were obtained with the imaginary parts very close to the wire model results. Compared with the free space case, all three poles are closer to the $j\omega$ axis of the complex plane as predicted in [4].

Both incident field and current density response waveforms were available from the ATLAS I test. This made it possible to divide out the incident field and compare directly with the Michigan data. The

frequency response at the midpoint of one wing with orientation 5 excitation was compared to the calculated wire model response and the Michigan scale model data. The graph is shown in Figure 31. The poles from data at two different locations were calculated and listed in Table 2. The interaction between the simulator structure and the test object in ATLAS I may be one reason for the differences in pole locations from that of the wire model. However, Lam's study [17] shows that the effect of this extra interaction is complicated. The normalization factor of the antisymmetric mode was calculated as $0.895 \times 10^6 + j\ 0.836 \times 10^5$ compared to $0.101 \times 10^7 + j\ 0.563 \times 10^5$ of the wire model. Overall, the results from ATHAMAS II and ATLAS I are very encouraging and argue in favor of taking more external data.

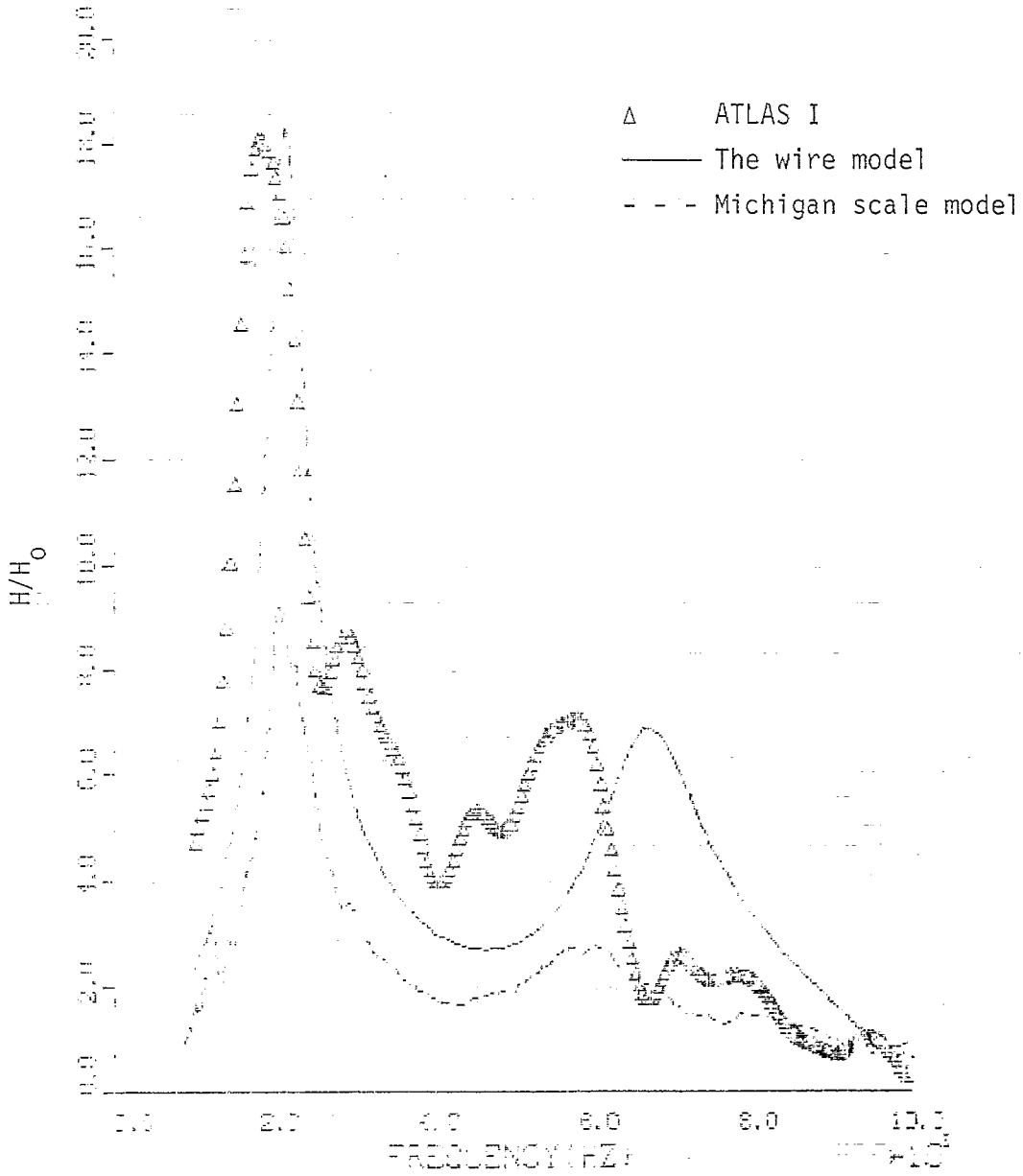

Figure 31. Frequency responses at the center of one wing with orientation 5 excitation from three data sources: the wire model, Michigan data, and ATLAS I.

CHAPTER 4

CONCLUSION AND RECOMMENDATIONS

The SEM parameters were calculated for a wire model of a B-52 aircraft. The results were compared with similar calculations using scale model data and system level test data. Several factors affect these comparisons:

(1) the wire model is a very simple model for an aircraft;

(2) both the wire model and scale model results are for free space conditions;

(3) the system level test data include simulator-test object interaction effects and

(4) only a small amount of measured data were available.

Despite these factors, the results indicate that the SEM representation can be applied to measured test data.

Because of cost, it is not practical to take enough system test measurements to completely define the SEM parameters for an aircraft. A reasonable approach is to present theoretical current density predictions and/or scale model data measurements as a collection of SEM parameters. These pretest data would be useful as a guideline for sensor placement and aircraft orientation in the system test. It would also be useful in making decisions about the "reasonableness" of the test results.

Once obtained, the system test data could be reduced to a collection of natural frequencies and (probably incomplete) modes

and coupling coefficients. This would provide a compact way of representing surface current density measurements and of comparing them with pretest predictions. It would also allow for a simple extrapolation technique--but this is a subject for future work.

REFERENCES

[1] C.E. Baum, "On the Singularity Expansion Method for the solution of Electromagnetic Interaction Problems," Interaction Note 88. Air Force Weapons Laboratory, Kirtland Air Force Base, NM, December 1971.

[2] T. T. Crow, B. D. Graves, and C. D. Taylor, "The Singularity Expansion Method as Applied to Perpendicular Crossed Cylinders in Free Space," Interaction Note 161. Air Force Weapons Laboratory, Kirtland Air Force Base, NM, October 1973.

[3] T. T. Crow, B. D. Graves, and C. D. Taylor, "Numerical Techniques Useful in the Singularity Expansion Method as Applied to Electromagnetic Interaction Problems," Mathematics Note 27. Air Force Weapons Laboratory, Kirtland Air Force Base, NM, December 1972.

[4] T. T.Crow, C. D. Taylor, and M. Kumbale, "The Singularity Expansion Method Applied to Perpendicular Crossed Wires Over a Perfectly Conducting Ground Plane," Sensor and Simulation Note 258. Air Force Weapons Laboratory, Kirtland Air Force Base, NM, June 1979.

[5] C. D. Taylor, T. T. Crow, and V. Naik, "A Study of the EMP Interaction with Aircraft Over an Imperfect Ground Plane," Interaction Note 362. Air Force Weapons Laboratory, Kirtland Air Force Base, NM, May 1979.

[6] G. Bedrosian, "Stick-Model Characterization of the Natural Frequencies and Natural Modes of the Aircraft," Interaction Note 326. Air Force Weapons Laboratory, Kirtland Air Force Base, NM, September 1977.

[7] V. Liepa, D. L. Senjupta, J. E. Ferris, and T. B. A. Senior, "Surface Field Measurements with Image and Ground Planes," Sensor and Simulation Note 244. Air Force Weapons Laboratory, Kirtland Air Force Base, NM, November 1977.

[8] F. B. Hildebrand, "Introduction to Numerical Analysis," McGraw-Hill, 1974.

[9] J. T. Cordaro, "Pole Measurements for the ATHAMAS Pipe Test," Mathematics Notes 56. Air Force Weapons Laboratory, Kirtland Air Force Base, NM, August 1977.

[10] A. G. Evans and R. Fischi, "Optimal Least Squares Time-Domain Synthesis of Recursive Digital Filters," IEEE Trans. on Audio and Electroacoustics; Vol. AU-21, February 1973.

[11] A. J. Poggio, E. K. Miller, and G. J. Burke, "An Integro-Differential Equation Technique for the Time-Domain Analysis of Thin Wire Structures, Part I--The Numerical Method," Journal of Computing Physics; Vol. 12, pp. 24-28, May 1973.

[12] A. J. Poggio, E. K. Miller, and G. J. Burke, "An Integro-Differential Equation Technique for the Time-Domain Analysis of Thin Wire Structures, Part II--Numerical Results," Journal of Computing Physics; Vol. 12, pp. 210-233, June 1973.

[13] J. A. Landt, E. K. Miller, and M. L. Van Blaricum, "A Computer Program for the Time-Domain Electromagnetic Response of Thin-Wire Structures," Interaction Note 210. Air Force Weapons Laboratory, Kirtland Air Force Base, NM, May 1974.

[14] C. E. Baum, "Interaction of Electromagnetic Fields with an Object Which Has an Electromagnetic Symmetry Plane," Interaction Note 63. Air Force Weapons Laboratory, Kirtland Air Force Base, NM, March 1971.

[15] A. G. Finci, T. K. Liu, and F. M. Tesche, "Determination of EMP Induced Axial Currents and Linear Charge Densities on a B-52 Aircraft Using the Stick Model Approach," Mission Research Corporation Report, June 1979.

[16] T. H. Shumpert, "Singularities, Coupling Coefficients and Mode Vectors for a Thin Wire Scatterer Parallel to a Lossy Ground." Auburn University Report, Auburn, Alabama, December 1979.

[17] J. Lam, "Interaction Between a Parallel-Plate EMP Simulator and a Cylindrical Test Object," Sensor and Simulation Note 264. Air Force Weapons Laboratory, Kirtland Air Force Base, NM, June 1979.

[18] K. S. Cho and J. T. Cordaro, "Calculation of the Singularity Expansion Method Parameters from the Transient Response of a Thin Wire," Interaction Note 379. Air Force Weapons Laboratory, Kirtland Air Force Base, NM, September 1979.

[19] K. T. Astrom and P. Eykhoff, "System Identification--A Survey," Automatica, Vol. 7, 1971.

[20] C. L. Lawson and R. J. Hanson, "Solving the Least Square Problems," Prentice-Hall, 1974.

APPENDIX

This appendix provides two algorithms used in this thesis for calculating poles and residues from transient time response, that is, "Prony's Method" [8], and the "Iterative Premultiply Method" [9], [10].

1. Prony's Method

For a system with only simple poles, the system's natural response can be expressed as

$$y(t) = \sum_{i=1}^{M} c_i \exp(s_i t) \tag{A.1}$$

where the s_i are the poles in the complex frequency plane, and the c_i are their corresponding residues. Since $y(t)$ is a real function of time, the s_i must either be real or occur in complex conjugate pairs. Let $y(t)$ be sampled at equal time intervals with a total of N points, then we can write

$$y(kT) = y_k = \sum_{i=1}^{M} c_i \exp(s_i kT); \quad k = 0, 1, \ldots, N-1 \tag{A.2}$$

where y_k are the sampled values and T is the sampling interval. (A.2) is rewritten as

$$y_k = \sum_{i=1}^{M} c_i z_i^k \; ; \; k = 0, 1, \ldots, N-1 \tag{A.3}$$

where $z_i = \exp(s_i T)$.

With this set of equations, the problem is to solve for both the

M values of z_i and the M values of c_i. It is assumed that the value of N be at least equal to 2M. The solution to this set of equations is nontrivial, since they are nonlinear in the z_i's. Let $z_1, z_2, \ldots, z_M$ be the roots of the algebraic equation

$$z^n + a_1 z^{n-1} + a_2 z^{n-2} + \cdots + a_{M-1} z + a_M = 0 \qquad (A.4)$$

so that the left-hand side of (A.4) is equal to the product

$$(z-z_1)(z-z_2) \cdots (z-z_M).$$

In order to determine the coefficients $a_1, a_2, \ldots, a_M$, we multiply the first equation in (A.3) by a_M, the second equation by $a_{M-1}, \ldots$, the M^{th} equation by a_1, the $(M+1)^{th}$ equation by 1, and add the results. Since each of the z_i satisfies (A.4), then the result is of the form

$$y_M + a_1 y_{M-1} + \cdots + a_M y_0 = 0$$

A set of N-M-1 additional equations of similar type is obtained in the same way by starting instead successively with the second, third, ..., $(N-M)^{th}$ equation. In this way it is possible to obtain the N-M linear difference equations

$$\begin{aligned}
&y_M + a_1 y_{M-1} + a_2 y_{M-2} + \cdots + a_M y_0 = 0 \\
&y_{M+1} + a_1 y_M + a_2 y_{M-1} + \cdots + a_M y_1 = 0 \\
&\quad\vdots \qquad\qquad\quad \vdots \qquad\qquad\qquad (A.5a) \\
&y_{N-1} + a_1 y_{N-2} + a_2 y_{N-3} + \cdots + a_M y_{N-M-1} = 0
\end{aligned}$$

which can be written in matrix form as

$$\underline{y} = H\,\underline{a} \tag{A.5b}$$

with

$$\underline{y} = \left[y_M \cdots y_{N-1}\right]^T$$

$$H = \begin{bmatrix} -y_{M-1} & \cdots & -y_0 \\ \cdot & & \cdot \\ \cdot & & \cdot \\ \cdot & & \cdot \\ -y_{N-2} & \cdots & -y_{N-M-1} \end{bmatrix}$$

$$\underline{a} = \left[a_1 a_2 \cdots a_M\right]^T$$

Since H and $\underline{y}$ are known, $\underline{a}$ can be found as

$$\underline{a} = H^{-1}\underline{y} \text{ , if } N = 2M \tag{A.6a}$$

or, if $N > 2M$, $\underline{a}$ can be obtained by the least square method as

$$\underline{a} = (H^T H)^{-1} H^T \underline{y} \tag{A.6b}$$

After $\underline{a}$ is determined, the M values of z_i can be found as the roots of (A.4). (A.3) then becomes a system of linear equations in the c_i with known coefficients. The c_i can be determined from the first M of these equations. It is trivial to obtain the poles s_i, since the roots of Equation (A.4) were defined by (A.3) as $z_i = \exp(s_i t)$, then the poles are simply

$$s_i = \frac{\ln z_i}{T} \tag{A.7}$$

In summary, the Prony's method, instead of attacking the nonlinear equations directly, solves two sets of linear equations and an M^{th}-order algebraic equation. Thus, the nonlinearity of the equations is concentrated in the single algebraic equation. Up to this point, the problem seems to be solved; however, when the transient response is corrupted by noise and the signal to noise is low, Prony's method has proven to be inaccurate [9], [18]. One way to overcome this difficulty is discussed in the next section.

2. Iterative premultiply method

When the data are measured by some measurement device, they are by no means noise free. Noise is also present in the analog to digital conversion and quantization process, which are necessary for digital processing. Let y_k, $k = 0, 1, \ldots, N-1$, be samples from an observed transient waveform. We want to approximate y_k by a sequence of the form

$$x_k = \sum_{i=1}^{M} c_i \exp(s_i kT) \; ; \; k = 0, 1, \ldots, N-1 \qquad (A.8)$$

For a given choice of the c_i, s_i, and M, there may be error between y_k and x_k, which is denoted by

$$e_k = y_k - x_k \qquad (A.9)$$

The mean squared error is defined by

$$E(M, c_i, s_i) = \frac{1}{N} \sum_{k=0}^{N-1} e_k^2 \qquad (A.10)$$

The values of c_i and s_i that minimized $E(M,c_i,s_i)$ for a fixed M are called the minimum mean squared error estimates. With this framework the problem of calculating poles and residues from a transient waveform can be stated in two parts: (1) find the minimum squared error estimates of c_i and s_i for a fixed M, and then (2) determine a "suitable" value of M.

From (A.5a) we can write

$$x_k + a_1 x_{k-1} + \cdots + a_M x_{k-M} = 0;\ N-1 \geq k \geq M \tag{A.11}$$

Using Equation (A.9) in Equation (A.11), we get the relation

$$y_k + a_1 y_{k-1} + \cdots + a_M y_{k-M} = e_k + a_1 e_{k-1} + \cdots + a_M e_{k-M};\ N-1 \geq k \geq M \tag{A.12}$$

Now let v_k be the right-hand side of (A.12). Then we have the matrix equation

$$\underline{y} = H\,\underline{a} + \underline{v} \tag{A.13}$$

where $$\underline{v} = \left[v_M, v_{M+1} \cdots v_{N-1}\right]^T$$

$\underline{y}$, H, and $\underline{a}$ are as defined in (A.5b).

When using Prony's method one obtains the same least squares solution as in Equation (A.6b), that is,

$$\underline{a}_{LS} = (H^T H)^{-1} H^T \underline{y} \tag{A.14}$$

This solution is a biased estimate of $\underline{a}$ unless the covariance matrix of $\underline{v}$ is a constant times the identity matrix [19]. In the case considered here the components of $\underline{v}$ are linear combinations of the error

e_k, k = 0, 1,...N-1. As a result the estimates of a_i are biased and the poles calculated from these estimates can be far from the estimates that minimize $E(M,c_i,s_i)$. In fact, these least squares solutions minimized $\underline{v}^T\underline{v}$, rather than $E(M,c_i s_i)$ that we want to minimize.

To derive the iterative premultiply algorithm, let us check the relation between e_k and v_k. From (A.13) we have

$$v_k = e_k + a_1 e_{k-1} + \cdots + a_k e_{k-M};\ N-1 \geq k \geq M \qquad (A.15)$$

Let

$$\underline{e} = \left[e_0 e_1 \cdots e_{N-1}\right]^T$$

and

$$D = \begin{bmatrix} a_M & \cdots & a_1 & 1 & 0 & \cdots & 0 \\ 0 & a_M & \cdots & a_1 & 1 & 0 & \cdots & 0 \\ \cdot & & & & & & & \cdot \\ \cdot & & & & & & & \cdot \\ \cdot & & & & & & & \cdot \\ 0 & \cdots & & a_M & \cdots & a_1 & 1 \end{bmatrix}$$

The matrix D is N-M-1 by N. Using this definition and (A.15), we can write

$$\underline{v} = D\,\underline{e} \qquad (A.16)$$

The error we would like to minimize is $\underline{e}^T\underline{e} = E(M,c_i,S_i)$. The matrix D is singular so we cannot solve for $\underline{e}$ directly, but by using the pseudo-inverse for D, it is easy to show [20] that the minimum norm solution of (A.16) satisfies

$$\underline{e}^T\underline{e} = \underline{v}^T(DD^T)^{-1}\underline{v} \qquad (A.17)$$

Using (A.13) and (A.17) we have

$$\underline{e}^T\underline{e} = (\underline{y} - H\underline{a})^T(DD^T)^{-1}(\underline{y} - H\underline{a}) \qquad (A.18)$$

This equation expresses the original error defined in (A.9) in terms of the difference equation parameters a_i, i=1, 2,...M. The problem of minimizing $E(M,c_i,S_i) = \underline{e}^T\underline{e}$ is then the problem of minimizing (A.18) with respect to the a_i. The equation is nonlinear, but a simple iterative technique can be used to find the minimum [10].

Suppose $\underline{e}$ is a vector of uncorrelated random variables, each with mean zero and variance one. Then from (A.16) the variance of $\underline{v}$, R_v will be

$$R_v = DD^T \qquad (A.19)$$

Using this expression for R_v, we can see that the minimum variance, unbiased estimate for $\underline{a}$ is given by (A.18). To motivate the technique for minimizing (A.18), we observe that if the matrix DD^T did not depend on $\underline{a}$, then the minimum of $\underline{e}^T\underline{e}$ would be given by the solution for $\underline{a}$ from the normal equation

$$H^T(DD^T)^{-1}H\underline{a} = H^T(DD^T)^{-1}\underline{y} \qquad (A.20)$$

Since D does in fact depend on $\underline{a}$, we can use (A.20) but with iterations. That is, we solve (A.20) for $\underline{a}$ with DD^T = Identity matrix, then compute DD^T from the estimated $\underline{a}$ and recompute $\underline{a}$ from (A.20). This process is continued until the estimate of $\underline{a}$ converges.

Equation (A.20) shows the inverse of DD^T. It is unnecessary and inefficient to compute this inverse, since DD^T is a symmetric positive

definite matrix. It can be factored with Cholesky's method [20] as

$$DD^T = F^TF \tag{A.21}$$

where F is upper triangular and nonsingular. Define $\underline{\tilde{y}}$ and $\tilde{H}$ as the solutions of the equations

$$\begin{aligned} F^T\underline{\tilde{y}} &= \underline{y} \\ F^T\tilde{H} &= H \end{aligned} \tag{A.22}$$

Using (A.22) in (A.20) we can get

$$\tilde{H}^T\tilde{H}\underline{a} = \tilde{H}^T\underline{\tilde{y}} \tag{A.23}$$

as the set of normal equations to be solved for $\underline{a}$.

To summarize, the iterative procedure consists of the following steps:

1. Solve Equation (A.20) for $\underline{a}$ with $DD^T = I$.
2. Compute DD^T from the present $\underline{a}$.
3. Factor DD^T and compute $\underline{\tilde{y}}$ and $\tilde{H}$.
4. Solve for a new $\underline{a}$ from (A.20).
5. Check if the new $\underline{a}$ has changed appreciably from the previous one. If yes, return to step 2. Otherwise the iteration is complete.

After $\underline{a}$ is obtained, the procedures to solve for s_i and c_i are the same as those in Prony's method discussed in the previous section.

The "suitable" number of poles, M, depends on the characteristics of the transient data. There is no easy formula for this determination. One practical way to use this iterative premultiply

method is to try it for several different values of M, and pick up those poles that are numerically stable as the poles of the system.

☆U.S. GOVERNMENT PRINTING OFFICE : 1981—576-115/519